HOKKAIDO UNIVERSITY

Title	Infrared spectra of isoquinolinium (iso-C9H7NH+) and isoquinolinyl radicals (iso-C9H7NH and 1-, 3-, 4-, 5-, 6-, 7- and 8-iso-HC9H7N) isolated in solid para-hydrogen
Author(s)	Joshi, Prasad Ramesh; Tsuge, Masashi; Tseng, Chih-Yu et al.
Citation	Physical Chemistry Chemical Physics, 25(17), 11934-11950 https://doi.org/10.1039/D3CP00246B
Issue Date	2023-02-20
Doc URL	https://hdl.handle.net/2115/91158
Type	journal article
File Information	Isoquinoline-rev.pdf

Hokkaido University Collection of Scholarly and Academic Papers : HUSCAP

Infrared spectra of isoquinolinium (*iso*-$C_9H_7NH^+$) and isoquinolinyl radicals (*iso*-C_9H_7NH and 1-, 3-, 4-, 5-, 6-, 7-, and 8-*iso*-HC_9H_7N) isolated in solid *para*-hydrogen

Prasad Ramesh Joshi,*[a] Masashi Tsuge,*[b] Chih-Yu Tseng,[a] and Yuan-Pern Lee*[ac]

[a] Department of Applied Chemistry and Institute of Molecular Science, National Yang Ming Chiao Tung Yang Ming University, Hsinchu 300093, Taiwan
[b] Institute of Low Temperature Science, Hokkaido University, Sapporo 060-0819, Japan
[c] Center for Emergent Functional Matter Science, National Yang Ming Chiao Tung University, Hsinchu 300093, Taiwan

E-mail: prasad.nctu@gmail.com, tsuge@lowtem.hokudai.ac.jp and yplee@nctu.edu.tw.
Orcid.org/0000-0003-0896-4341 (PRJ)
Orcid.org/0000-0001-9669-1288 (MT)
Orcid.org/0000-0001-6418-7378 (YPL)

KEY WORDS: Infrared spectroscopy, isoquinoline, isoquinolinium, isoquinolinyl radicals, *para*-hydrogen, matrix isolation

ABSTRACT

Protonated polycyclic aromatic nitrogen heterocycles (H^+PANH) are prospective candidates that might contribute to the interstellar unidentified infrared (UIR) emission bands because protonation enhances the relative intensities of bands near 6.2, 7.7, and 8.6 μm and the presence of N atom induces a blue shift of the ring-stretching modes so that the spectra of H^+PANH match better with the 6.2-μm feature in the class-A UIR spectra. We report the infrared (IR) spectra of protonated isoquinoline (2-isoquinolinium cation, *iso*-$C_9H_7NH^+$), its neutral counterpart (2-isoquinolinyl radical, *iso*-C_9H_7NH), and another mono-hydrogenated product (6-isoquinolinyl radical, 6-*iso*-HC_9H_7N), produced on electron-bombardment of a mixture of isoquinoline (*iso*-C_9H_7N) with excess *para*-hydrogen (*p*-H_2) during matrix deposition at 3.2 K. To generate additional isomers of hydrogenated isoquinoline, we irradiated *iso*-$C_9H_7N/Cl_2/p$-H_2 matrices at 365 nm to generate Cl atoms, followed by IR irradiation to generate H atoms via Cl + H_2 (v = 1) → HCl + H; the H atoms thus generated reacted with *iso*-C_9H_7N. In addition to *iso*-C_9H_7NH and 6-*iso*-HC_9H_7N observed in electron-bombardment experiments, we identified six additional hydrogenated isoquinoline, 1-, 3-, 4-, 5-, 7-, and 8-*iso*-HC_9H_7N via their IR spectra; hydrogenation on the N atom and all available carbon atoms except two sharing carbon atoms on the fused ring were observed. Spectral groupings were achieved according to their behaviors after maintenance of the matrix in darkness and on secondary photolysis at varied wavelengths. The assignments were supported by comparison of experimental results with vibrational wavenumbers and IR intensities of possible isomers predicted with the B3LYP/6-311++G(d,p) method. The implication in the identification of the UIR band is discussed.

1. Introduction

The infrared (IR) emission from many astrophysical objects, showing common major features near 3.3, 6.2, 7.7, 8.6, and 11.2 μm, is referred to as the unidentified infrared (UIR) emission bands.[1,2] Because these emitting wavelengths are characteristic of the CH-stretching, CC-stretching, and CH-bending modes of aromatic compounds, IR fluorescence of polycyclic aromatic hydrocarbons (PAH) upon ultraviolet (UV) excitation has been proposed to be responsible for these UIR bands.[3−6] The slight variations in spectral patterns of UIR features among various interstellar objects are presumably due to distinct distributions of a group of emitters. Although laboratory IR spectra have been acquired for a number of PAH and their derivatives, no PAH has been positively identified as a carrier of the UIR bands. One of the discrepancies between IR spectra of neutral PAH and UIR bands lies in the relative intensities of bands; the intensities for features of neutral PAH near 6.2, 7.7 and 8.6 μm relative to other bands are smaller than those in UIR emission. Theoretical studies suggested that the intensity of these features is enhanced in ions of PAH, such as PAH cations and protonated PAH (designated H^+PAH).[7,8] We have experimentally demonstrated that IR spectra of relatively large H^+PAH, such as protonated coronene ($C_{24}H_{13}^+$),[9] protonated ovalene ($C_{32}H_{15}^+$),[10] and non-planar protonated corannulene ($C_{20}H_{11}^+$),[11] show such an enhancement and an improved agreement with the UIR emission spectra.[12]

Peeters et al.[13] reported that the UIR emission spectra can be classified as classes A, B, and C according to the band positions and the width of the individual bands in the wavelength region 6–9 μm. The feature near 6.2 μm in class-A spectra is asymmetric, with a maximum near 6.22 μm. This band position does not match the laboratory spectra of neutral PAH with a band near 6.3 μm, especially after accounting for the expected red shift ~15 cm^{-1} in converting the absorption spectra to UV-induced emission spectra.[7,14,15] The bands of H^+PAH near 6.3 μm associated with the CC-

stretching modes also mismatch with the feature near 6.2 μm in class-A UIR spectra. The substitution of a CH moiety with a nitrogen atom in PAH, known as polycyclic aromatic nitrogen heterocycles (PANH), was suggested to induce a blue shift of the CC-stretching bands of PAH near 6.3 μm so that it matches better with the UIR band near 6,2 μm.[13,15,16] The existence of PANH in interstellar media is plausible because nitrogen is the most abundant elements after hydrogen, helium, and carbon. Nitrogen-containing heterocycles are considered as key chemical species associated with the origin of life.[17] Small PANH, such as quinoline (C_9H_7N), isoquinoline (*iso*-C_9H_7N), and their derivatives, have been detected in meteorites;[18,19] possible mechanisms for the formation of small PANH have been discussed in the literature.[20]

Because of a large proton affinity at the nitrogen site, PANH can be protonated readily by H_3^+, which is abundant in interstellar space. For example, the proton affinity of quinoline is 953 kJ mol^{-1}, which is much greater than a value 803 kJ mol^{-1} of naphthalene.[21] The protonated PANH (designated H^+PANH) are considered to be a potentially important class of molecules responsible for UIR bands because protonation enhances the intensity of 6.2, 7.7, and 8.6 μm features and because the spectra of H^+PANH match better with the 6.2-μm feature in class-A UIR spectra.[13,15,16] Infrared multiphoton dissociation (IRMPD) spectra of some small $PANH^+$ and H^+PANH have been reported,[22] but the spectra were broad and were typically recorded only in spectral region 600–1600 cm^{-1}.

We have developed a technique to produce protonated and hydrogenated PAH, of which *para*-hydrogen (*p*-H_2) containing a small amount of PAH were bombarded with electrons during deposition at 3.2 K.[12,23,24,25] The ionization of H_2 molecule led to the formation of H_3^+ and H atom, which subsequently produced protonated species via proton transfer and their neutral counterparts, i.e., hydrogenated species, via neutralization and hydrogen reactions. Alternatively, for the

production of mono-hydrogenated PAH, we developed an efficient method to study hydrogenation reactions in solid *p*-H_2.[12,23,24,25,26] In this method, a Cl_2-doped PAH/*p*-H_2 matrix was initially photolyzed at 365 nm to generate Cl atom, followed by IR irradiation to generate H atoms via Cl + H_2 ($v = 1$) $\rightarrow$ HCl + H; H atoms are extremely mobile in quantum-solid *p*-H_2 as they can diffuse through the matrix via quantum tunneling. This method produced hydrogenated species with significantly improved efficiency over those from electron-bombardment experiments. Our methods have demonstrated several advantages over other techniques such as the IRMPD and infrared photodissociation (of tagged species).[12,23,24] Our techniques allow the production of protonated and hydrogenated species with little fragmentation. Because we measured IR absorption spectra of species isolated in *p*-H_2, the spectra are characterized by narrow lines with reliable relative IR intensities. A wider spectral coverage, 500–4000 cm^{-1}, allows us to identify lines associated with the CH- and NH-stretching modes as well. In the investigation of the IR spectra of H^+PANH, information on the NH-stretching and CH-stretching modes provides a definitive identification of isomers. Recently, our laboratory reported the IR spectrum of protonated quinoline (1-quinolinium cation, $C_9H_7NH^+$) in solid *p*-H_2.[25] We observed a line of the NH-stretching mode at 3385 cm^{-1}, four lines of ring-stretching modes in region 1400–1650 cm^{-1}, three lines of in-plane CH bending modes in region 1150–1300 cm^{-1}, and one line of out-of-plane CH bending mode at 790 cm^{-1}, which is much informative as compared with three broad bands identified with the IRMPD method near 1548, 1354, and 772 cm^{-1}.[22] The observed lines at 1641.4, 1598.4, and 1562.0 cm^{-1} were found to be blue-shifted from lines at 1618.7, 1580.8, 1556.7, and 1510.0 cm^{-1} of the corresponding protonated naphthalene ($C_{10}H_9^+$),[27] matching better with the 6.2-μm band of UIR emission. Furthermore, five isomers of quinolinyl radicals (C_9H_7NH and 3-, 4-, 7-, and 8-HC_9H_7N) were characterized by their IR spectra.

In this work, we extended our investigation to isoquinoline, which is a structural isomer of quinoline. In isoquinoline, the CH group at site 2 of naphthalene is substituted with a nitrogen atom (Fig. 1); the CH at site 1 is substituted with a nitrogen atom in quinoline. Isoquinoline has 10 possible protonation sites and the numbering of the sites are indicated in Fig. 1. In this paper, the isoquinoline protonated or hydrogenated at the N-atom site is designated as *iso*-$C_9H_7NH^+$ or *iso*-C_9H_7NH, respectively, and those protonated or hydrogenated at the C-atom sites of isoquinoline are designated as *n*-*iso*-$H^+C_9H_7N$ or *n*-*iso*-HC_9H_7N, in which *n* refers to the carbon number. When no specific isomeric form is referred, we designated the protonated and hydrogenated species as *iso*-$C_9H_8N^+$ and *iso*-C_9H_8N, respectively. The IRMPD spectrum of *iso*-$C_9H_7NH^+$ has been reported, but, as aforementioned, the spectral region is limited to 600–1600 cm^{-1}.[22] The spectral identification of *iso*-$C_9H_7NH^+$ was mostly based on an intense band at 774 cm^{-1} associated with the out-of-plane CH-bending mode and two other bands at 1360 and 1582 cm^{-1}; the characteristic NH-stretching band expected near 3400 cm^{-1} was unreported. Electronic excitation spectra of the $S_1 \leftarrow S_0$ and $S_3 \leftarrow S_0$ transitions of *iso*-$C_9H_7NH^+$ were reported; the spectra were characterized by band origins near 27500 and 42500 cm^{-1}, respectively, and a progression with spacing ~500 cm^{-1} associated with the Franck-Condon-active ring-deformation mode.[28,29]

Here, we report the IR identification of *iso*-$C_9H_7NH^+$ (2-isoquinolinium cation) and two isomers of isoquinolinyl radicals (*iso*-C_9H_7NH and 6-*iso*-HC_9H_7N) in solid *p*-H_2 produced in the electron-bombardment experiments. With the hydrogenation technique using Cl_2, we observed an unprecedented number of isomers of hydrogenated isoquinoline in one experiment. Infrared spectra of eight isomers of isoquinolinyl radicals, including *iso*-C_9H_7NH and 1-, 3-, 4-, 5-, 6-, 7-, and 8-*iso*-HC_9H_7N, were identified; hydrogenation on the N atom and all available C atoms except the two sharing carbon atoms in the fused ring was observed. The implication in the identification

of the UIR band is discussed.

2. Experiments

The IR absorption technique applied to species isolated in *p*-H_2 matrices has been described elsewhere.[12,23,24,25] A gold-plated copper substrate for matrix samples was cooled to 3.2 K by a closed-cycle helium refrigerator; it also served as a reflector for IR probing light to have reflective absorption. Absorption spectra were recorded with a Fourier-transform infrared (FTIR) spectrometer (Bruker, VERTEX 80V, KBr beam splitter, Hg-Cd-Te detector cooled to 77 K). Typically, 200 scans at resolution 0.25 cm^{-1} were recorded after each stage of the experiment.

The method for converting *normal*-H_2 (*ortho*-H_2 : *p*-H_2 = 3 : 1) to *p*-H_2 has been described previously.[12,23,24] Briefly, *normal*-H_2 was introduced into a copper cell filled with a catalyst (hydrated iron(III) oxide, 30–50 mesh) cooled to 12–13 K with another closed-cycle helium refrigerator. The proportion of *ortho*-H_2 in the resultant *p*-H_2 gas was typically less than 100 ppm. The isoquinoline sample was obtained commercially (97%, Acros organics) and degassed with several freeze–pump–thaw cycles.

Gaseous mixtures of *iso*-C_9H_7N/*p*-H_2 was prepared by flowing *p*-H_2 (flow rate ~10 mmol h^{-1}) over a flask containing liquid isoquinoline. The supply of *iso*-C_9H_7N vapor was controlled with a needle valve. The mixture was deposited onto the Cu substrate over a period of 7–8 h. During the deposition, the matrix was bombarded with an electron beam (20 μA current and 300 eV kinetic energy) to produce protonated and hydrogenated products. To differentiate various products produced by electron bombardment, the matrix was typically maintained in darkness for ~10 h, followed by secondary photolysis with light at 365 ± 10 nm from a light-emitting diode (375 mW) and at 405 nm from a diode laser (120 mW).

Alternatively, the isoquinolinyl radicals were produced in *iso*-$C_9H_7N/Cl_2/p$-H_2 matrices on UV photolysis at 365 nm for 1 h, followed by IR irradiation from an external globar source for 2 h. Secondary photolysis at 553, 540, 420, 405, and 365 nm (45–60 mW) using an OPO laser (EKSPLA, NT340, 10 Hz) were performed to distinguish various groups of lines according to their photolytic behavior. To avoid the reaction between Cl and *p*-H_2 during the IR spectral acquisition, an IR filter with cutoff wavelength at 2.4 μm was employed.

Because of the low vapor pressure of isoquinoline and the mixing method employed, we were unable to determine accurately the mixing ratio of *iso*-C_9H_7N/p-H_2 based on partial pressures. Instead, we estimated the mixing ratios according to the method developed by Tam and Fajardo.[30] The mixing ratio x (in ppm) of a species in solid *p*-H_2 is represented as

$$x = \frac{2.303 \int \log_{10}(I/I_0) d\nu}{\varepsilon\, l} \times V_m \times 10^6, \qquad (1)$$

in which ε is the absorption coefficient in cm mol^{-1}, $\int \log_{10}(I/I_0) d\nu$ is the observed integrated absorbance of a specific line, l (in cm) is the IR absorption path length through solid *p*-H_2, and V_m (= 23.16 cm^3 mol^{-1})[31] is the molar volume of solid *p*-H_2. Infrared absorption path length l was estimated from the integrated band area of transition $S_1(0) + S_0(0)$ in 4828–4853 cm^{-1} and pure rotational transition at 1167 cm^{-1} of the *p*-H_2 matrix.[32] Infrared intensities of a specific vibrational transition calculated with the B3LYP/6-311++G(d,p) method were used for ε; the error in calculated ε, hence x, might be as large as a factor of 2. By using several lines of the same species reduced the error in the estimated mixing ratio.

3. Quantum-chemical calculations

Quantum-chemical calculations were performed using the Gaussian 16 (Rev. B.01) program package.[33] Geometrical optimizations and vibrational analyses were performed with the B3LYP hybrid functionals [34, 35] and standard basis set 6-311++G(d,p). [36] Anharmonic vibrational

wavenumbers and IR intensities were calculated by employing a second-order vibrational perturbation theory (VPT2) implemented in Gaussian 16.[37] Furthermore, calculations on single-point electronic energies with the method coupled cluster with single and double and perturbative triple excitations, CCSD(T),[38] were performed on geometries obtained with the B3LYP/6-311++G(d,p) method; zero-point vibrational energies (ZPVE) were corrected according to the harmonic vibrational wavenumbers calculated with the B3LYP method. Calculations on the electronic excitation and oscillator strength were performed with time-dependent density-functional theory (TD-DFT) using the B3LYP/6-311++G(d,p) method.

3.1. Protonated isoquinoline (isoquinolinium cation)

Isoquinoline has 10 possible sites for protonation and the numbering of carbon and nitrogen atoms of isoquinoline is indicated in Fig. 1; N atom is numbered as 2 and the two sharing carbon atoms in the fused ring as 4a and 8a. The geometries of all isomers of protonated isoquinoline, with relative energies and representative geometrical parameters predicted with the CCSD(T)/6-311++G(d,p)//B3LYP/6-311++G(d,p) method, are presented in Fig. S1, ESI†. The isomer protonated at the N-atom site of isoquinoline, 2-isoquinolinium (*iso*-$C_9H_7NH^+$), was predicted to have the least energy; the energy of *iso*-$C_9H_7NH^+ + H_2$ is smaller than *iso*-$C_9H_7NH + H_3^+$ by 538 and 534 kJ mol^{-1}, implying a calculated proton affinity of 957 and 989 kJ mol^{-1} for *iso*-C_9H_7N on the N-atom site at the B3LYP and CCSD(T) levels, respectively. The energies of isomers protonated at the C-atom site of isoquinoline, 1-, 3-, 4-, 5-, 6-, 7-, and 8-*iso*-$H^+C_9H_7N$, are predicted to be 200, 190, 169, 171, 209, 183, and 190 kJ mol^{-1} greater than *iso*-$C_9H_7NH^+$, respectively, much smaller than values 267 and 240 kJ mol^{-1} predicted for 4a- and 8a-*iso*-$H^+C_9H_7N$, respectively (Table 1). In all isomers except 4a- and 8a-*iso*-$H^+C_9H_7N$, all carbon and nitrogen atoms remain in a plane and have symmetry of point-group C_s; the ring skeleton of 4a- and 8a-*iso*-$H^+C_9H_7N$ are

non-planar so that these two species belong to point group C_1. The proton-transfer reactions from H_3^+ to isoquinoline, $H_3^+ + iso\text{-}C_9H_7N \rightarrow H_2 + iso\text{-}C_9H_8N^+$, are barrierless. The potential energy scheme for the proton transfer among these isomers via moving toward the neighboring atom is presented in Fig. S2, ESI†. Although the energies of transition states for isomerization, 231–297 kJ mol^{-1}, are smaller than $H_3^+ + iso\text{-}C_9H_7N$ (534 kJ mol^{-1}), isomerization to other isomers is unlikely to occur once a product is stabilized in solid p-H_2.

The scaled harmonic and anharmonic vibrational wavenumbers and IR intensities for *iso*-$C_9H_7NH^+$ (Table S1, ESI†), 1-, 3-, and 4-*iso*-$H^+C_9H_7N$ (Table S2, ESI†), 5-, 6-, and 7-*iso*-$H^+C_9H_7N$ (Table S3, ESI†), and 8-, 4a-, and 8a-*iso*-$H^+C_9H_7N$ (Table S4, ESI†) are listed. The scaling of harmonic vibrational wavenumbers is discussed in Section 4.1. The stick spectra in region 1800–600 cm^{-1} for all isomers of protonated isoquinoline, simulated according to scaled harmonic wavenumbers and IR intensities, are presented in Fig. S3, ESI†.

3.2. Hydrogenated isoquinoline (isoquinolinyl radical)

The geometries of all isomers of mono-hydrogenated isoquinoline (*iso*-C_9H_8N, isoquinolinyl radical), with key geometrical parameters and relative energies predicted with the CCSD(T)/6-311++G(d,p)//B3LYP/6-311++G(d,p) method, are presented in Fig. S4, ESI†. The isomer hydrogenated at the N-atom site, 2-isoquinolinyl radical (*iso*-C_9H_7NH), was predicted to have the least energy, −111 kJ mol^{-1} relative to H + *iso*-C_9H_7N. The energies of other isomers, 1-, 3-, 4-, 5-, 6-, 7-, and 8-*iso*-HC_9H_7N, are predicted to be 6, 22, 3, 2, 24, 24, and 3 kJ mol^{-1}, respectively, relative to *iso*-C_9H_7NH. The corresponding values for 4a- and 8a-*iso*-HC_9H_7N are much greater, 100 and 91 kJ mol^{-1}, respectively. In all isomers except 4a- and 8a-*iso*-HC_9H_7N, carbon and nitrogen atoms remain planar and have symmetry of point-group C_s; 4a- and 8a-*iso*-HC_9H_7N have non-planar ring skeleton and belong to point group C_1. The calculated barriers for H-atom addition,

H + *iso*-C_9H_7N → *iso*-C_9H_8N, and those for hydrogen transfer to the neighboring site are presented in Fig. S5, ESI†. All barrier heights for reactions H + *iso*-C_9H_7N → *iso*-C_9H_8N are smaller than 27 kJ mol^{-1}, except those for the formation of 4a- and 8a-*iso*-HC_9H_7N, which have barriers > 46 kJ mol^{-1} (Table 1). Because the energies of TS for isomerization are greater than that of H + *iso*-C_9H_7N, isomerization reactions will not occur during hydrogenation of isoquinoline in the low-temperature solid *p*-H_2 environment.

The harmonic and anharmonic vibrational wavenumbers and IR intensities for *iso*-C_9H_7NH, 1-, and 3-*iso*-HC_9H_7N (Table S5, ESI†), 4-, 5-, and 6-*iso*-HC_9H_7N (Table S6, ESI†), 7- and 8-*iso*-HC_9H_7N (Table S7, ESI†), and 4a- and 8a-*iso*-HC_9H_7N (Table S8, ESI†) are listed. The IR stick spectra in region 1800–600 cm^{-1} for all isomers of hydrogenated isoquinoline, simulated according to the scaled harmonic vibrational wavenumbers and IR intensities, are presented in Fig. S6, ESI†.

4. Experimental results

4.1 IR spectrum of *iso*-C_9H_7N/*p*-H_2 matrices

An IR spectrum recorded after deposition of a *iso*-C_9H_7N/*p*-H_2 mixture for 5 h is presented in Fig. S7a, ESI†. Intense lines were observed at 3069.6, 1632.8, 1595.0, 1273.0, 826.3, 740.1, and 481.0 cm^{-1}, with the most intense line at 826.3 cm^{-1}. On comparison of observed vibrational wavenumbers and relative intensities with calculations, we assigned 24 observed lines to the fundamental vibrational transitions of *iso*-C_9H_7N. The observed vibrational wavenumbers are plotted against the harmonic vibrational wavenumbers predicted with the B3LYP/6-311++G(d,p) method in Fig. S8, ESI†. A linear regression yielded satisfactory linear relation with a scaling equation $y = (0.9823 \pm 0.0025)\, x + (0.6 \pm 2.8)$ for wavenumbers 600−2000 cm^{-1}, in which y is the scaled vibrational wavenumber and x is the calculated harmonic vibrational wavenumber; the errors present one standard deviation in fitting. For lines with wavenumbers above 2000 cm^{-1},

assignments for *iso*-C_9H_7N are difficult because of severe interactions of the CH-stretching modes with some overtone or combination modes. We hence adopted the equation for quinoline in *p*-H_2, $y = 0.9122\ x + 174.3$;[25] the error in this region is hence expected to be greater. We used these equations to scale the harmonic vibrational wavenumbers predicted for *iso*-C_9H_7N, *iso*-$C_9H_8N^+$, and *iso*-C_9H_8N.

Simulated stick spectra according to scaled harmonic and anharmonic vibrational wavenumbers are presented in Figs. S7b and S7c, ESI†, respectively. The observed and predicted wavenumbers and relative intensities are summarized in Table S9, ESI†. The mean absolute deviation between observed and scaled harmonic vibrational wavenumbers is 6.5 ± 9.4 cm^{-1}; that between observed and anharmonic vibrational wavenumbers is 8.8 ± 10.9 cm^{-1}, indicating a satisfactory agreement between experimental and predicted vibrational wavenumbers.

The absorption path length of the matrix (*l* in Eq. 1) was estimated to be ~1.0 mm. Using the integrated absorbance of lines at 1632.8, 1595.0, 826.3, and 740.1 cm^{-1}, we derived a mixing ratio 54 ± 2 ppm for *iso*-C_9H_7N/*p*-H_2 in Fig. S7a, ESI†; listed error represents one standard deviation among mixing ratios estimated from each absorption line.

4.2 IR spectra of electron-bombarded *iso*-C_9H_7N/*p*-H_2 matrices

Figure 2 shows IR spectra of an electron-bombarded *iso*-C_9H_7N/*p*-H_2 matrix in spectral regions 3550–3370 and 1670–600 cm^{-1}. Figure 2a presents the spectrum recorded after deposition of electron-bombarded matrix for 7 h, with lines of *iso*-C_9H_7N stripped using Fig. S7a, ESI†. Therefore, the positive lines in this spectrum are induced by electron bombardment. Figure 2b shows the difference spectrum after maintaining the matrix in darkness for 10 h; positive lines indicate generation and negative lines indicate destruction. After this experimental step, the matrix was irradiated at 365 nm for 25 min followed by 405 nm for 3 h. The difference spectra after each

secondary irradiation step are shown in Figs. 2c and 2d.

It has been demonstrated that electron bombardment during deposition of a *p*-H_2 matrix containing the guest molecules produces protonated and hydrogenated products.[12,23,24] During maintenance of the deposited matrix in darkness for a prolonged period, electrons trapped in solid *p*-H_2 slowly diffused to neutralize protonated products and produce their neutral counterparts. The trapped hydrogen atoms (i.e., those unreacted during deposition) might further react with parent molecules to produce hydrogenated products. Consequently, during maintenance in darkness, the intensities of lines of protonated species and the parent molecules are expected to decrease, while those of hydrogenated species increase. In the spectra shown in Fig. 2, we identified several groups of lines (groups A^+, A, and B) according to their characteristic behavior after each experimental step. The intensities of lines in group A^+ decreased after maintaining the matrix sample in darkness for 10 h (Fig. 2b). Those increased at this step was further classified into two groups according to their behavior upon secondary irradiation at 365 and 405 nm. The intensities of lines in groups A and B decreased by similar proportions, 40–50 %, upon irradiation at 365 nm (Fig. 2c), whereas those of lines in group B further decreased by 35 % upon irradiation at 405 nm (Fig. 2d); the percentage is based on the spectrum measured after maintaining the matrix sample in darkness for 10 h.

Lines in group A^+ include intense features observed at 3397.2, 1643.3, 1400.1, 1378.6, and 791.4 cm^{-1} and weaker ones at 1554.7 and 1497.3 cm^{-1}; a line at 720.0 cm^{-1} might also belong to this group, but it was severely interfered with by the absorption of *p*-H_2. The vibrational wavenumbers and integrated relative intensities of these lines are listed in Table 2. To be discussed in Section 5.1, these lines in group A^+ are assigned to *iso*-$C_9H_7NH^+$ (2-isoquinolinium cation). Lines in group A include intense lines at 3495.2, 3491.0, 1613.9, 1476.6, 1440.5, 1180.9, 988.3,

763.1, and 737.3 cm^{-1} and seven weaker lines, with the most intense line at 988.3 cm^{-1}. These lines in group A are assigned to *iso*-C_9H_7NH (2-isoquinolinyl radical), to be discussed in Section 5.2. Lines in group B include intense lines at 1557.5, 1446.8, 1284.5, 890.9, 810.2, and 697.3 cm^{-1}, with the most intense line at 810.2 cm^{-1}, and several weaker ones. To be discussed in Section 5.2, these lines in group B are assigned to 6-*iso*-HC_9H_7N (6-isoquinolinyl radical). Lines in groups A and B were also observed in hydrogenation experiments, to be described in Section 4.3.

4.3 IR spectra of UV/IR irradiated *iso*-$C_9H_7N/Cl_2/p$-H_2 matrices

Figure 3a depicts the IR spectrum in region 1200–600 cm^{-1}, recorded after photolysis at 365 nm for 1 h of an *iso*-$C_9H_7N/Cl_2/p$-H_2 matrix deposited for 8 h. The corresponding IR spectra covering 3600–3470, 3100–2700, and 1700–1200 cm^{-1} are presented in Fig. S9, ESI†. Upon photolysis at 365 nm, no new features were observed, except weak lines at 1441.1 cm^{-1} (assigned to ClOO due to the reaction of Cl with trace O_2 impurity)[39] and at 943.8 cm^{-1} (the spin-orbit transition of Cl),[40] indicating the production of Cl atoms. This matrix was further exposed to IR irradiation for 2 h; the difference spectrum is shown in Fig. 3b. In addition to those described in the previous section for groups A and B, many new lines were observed. To differentiate these newly observed features, secondary irradiation at 553, 540, 420, 405, and 360 nm was performed sequentially for 30 min at each wavelength; the difference spectra after each step are presented in Figs. 3c–3g, respectively.

According to the distinct behavior on secondary photolysis at varied wavelengths, we categorized newly observed features after IR irradiation into eight groups, designated as groups A to H; their photolytic behaviors are summarized in Table 3; the listed percentage variations are based on the spectrum measured after IR irradiation. Results from secondary irradiation at 420 and 405 nm are the most informative because intensity variations of lines were observed in almost all

groups except groups G and H at 420 nm and group E at 405 nm, but information from irradiation at other wavelengths was also required to differentiate each group. At 420 nm, lines in groups A, B, C, and E decreased, whereas those in groups D and F increased. At 405 nm, those in groups A, B, C, and H decreased, whereas those in groups D, F, and G increased. The distinct features of eight groups are indicated with color-coded arrows and group labels in Fig. 3 and Fig. S9, ESI†. These features in groups A−H are assigned to *iso*-C_9H_7NH and 6-, 7-,8-, 4-, 5-, 1-, and 3-*iso*-HC_9H_7N, respectively, to be discussed in Sections 5.2−5.5.

We integrated several intense lines in each group, as listed in Table S10, ESI†, to estimate the mixing ratios after UV/IR irradiation of the *iso*-C_9H_7N/Cl_2/*p*-H_2 matrices. The estimated mixing ratios are [*iso*-C_9H_7N] = (90 ± 12) ppm, [*iso*-C_9H_7NH] = (2.8 ± 0.5) ppm, [6-*iso*-HC_9H_7N] = (2.1 ± 1.2) ppm, [7-*iso*-HC_9H_7N] = (1.1 ± 0.4) ppm, [8-*iso*-HC_9H_7N] = (1.6 ± 0.1) ppm, [4-*iso*-HC_9H_7N] = (2.5 ± 0.3) ppm, [5-*iso*-HC_9H_7N] = (1.5 ± 0.3) ppm, [1-*iso*-HC_9H_7N] = (1.5 ± 0.3) ppm, and [3-*iso*-HC_9H_7N] = (0.42 ± 0.01) ppm; listed errors represent one standard deviation among various lines.

5. Discussion

5.1 Assignment of lines in group A^+ to 2-isoquinolinium cation (*iso*-$C_9H_7NH^+$)

As aforementioned, during maintenance of electron-bombarded matrix in darkness, electrons trapped in solid *p*-H_2 will slowly diffuse and neutralize cationic species. The intensities of the lines in group A^+ decayed during this process, indicating that the most likely carrier of lines in this group is isoquinolinium cation, i.e., protonated isoquinoline. In Fig. 4a, we reproduced Fig. 2a, the IR spectrum of the electron-bombarded matrix with absorption lines of *iso*-C_9H_7N stripped, and indicated lines in group A^+ with arrows and labels; the regions subjected to interference by intense absorption of the precursor (*iso*-C_9H_7N) and other products are shaded gray. The stick spectrum of

iso-$C_9H_7NH^+$ simulated according to scaled harmonic vibrational wavenumbers and IR intensities is presented in Fig. 4b.

The observed wavenumbers and relative integrated intensities of lines in group A^+ agree the best with those predicted for *iso*-$C_9H_7NH^+$, as compared in Table 2. The most intense line observed at 3397.2 cm^{-1} is characteristic of the N–H stretching mode; the observed wavenumber agrees satisfactorily with the scaled harmonic vibrational wavenumber 3430 cm^{-1} (with intensity 208 km mol^{-1}) and anharmonic vibrational wavenumbers at 3407 cm^{-1} for the N–H stretching mode of *iso*-$C_9H_7NH^+$. The C−H stretching modes of *iso*-$C_9H_7NH^+$ have IR intensities less than 8 km mol^{-1} and were severely interfered by precursor absorption, so they could not be definitively identified. Similarly, for all C-protonated isomers except 4a- and 8a-*iso*-$H^+C_9H_7N$, the C−H stretching modes of *iso*-$H^+C_9H_7N$ are weak and only the CH_2 symmetric stretching mode, predicted in the region 2800–2900 cm^{-1} has intensity 32−91 km mol^{-1}. For 4a- and 8a-*iso*-$H^+C_9H_7N$, the new C−H stretching mode on the fused ring is predicted near 2650 cm^{-1} with intensity ~50 km mol^{-1}. However, no new lines that were induced by electron bombardment and decayed after maintenance in darkness were observed in the 2650−2900 cm^{-1} region.

In the region below 1700 cm^{-1}, four intense lines were observed at 1643.3, 1400.1, 1378.6, and 791.4 cm^{-1}, near the scaled harmonic wavenumbers predicted for *iso*-$C_9H_7NH^+$ at 1639 (ν_9, N-containing ring stretch), 1394 (ν_{16}, ring stretch), 1382 (ν_{17}, ring stretch), and 788 (ν_{40}, out-of-plane C–H and N–H bend) cm^{-1}, respectively. Weaker lines observed at 1554.7 and 1497.3 cm^{-1} correspond to 1559 (ν_{12}, ring stretch) and 1500 (ν_{13}, ring stretch) cm^{-1}, respectively. Other relatively intense lines of *iso*-$C_9H_7NH^+$ at 1620 (ν_{10}), 1587 (ν_{11}), 1285 (ν_{18}), and 471 (ν_{44}) cm^{-1} were predicted to have IR intensities 27, 15, 13, and 29 km mol^{-1}, respectively. These lines could not be identified definitively because of the spectral interference from the intense absorption of

the parent. The mean absolute deviation between observed and scaled harmonic vibrational wavenumbers is 8.3 ± 10.0 cm^{-1}, which improves to 4.2 ± 1.0 cm^{-1} on excluding the N–H stretching mode (ν_1). The deviation between observed and anharmonic wavenumbers is 9.8 ± 6.6 cm^{-1}, which does not change significantly (9.7 ± 7.2 cm^{-1}) after excluding ν_1. These results indicate a satisfactory agreement between experiments and predicted vibrational wavenumbers of *iso*-$C_9H_7NH^+$. The comparison of lines in group A^+ with the predicted spectra of all isomers of protonated isoquinoline (*iso*-$C_9H_8N^+$) is presented in Figs. S10 and S11, ESI†; the observed spectrum of group A^+ agree poorly with the stick IR spectra simulated for isomers of isoquinoline protonated at a carbon site, i.e., 1-, 3-, 4-, 5-, 6-, 7-, 8-, 4a-, and 8a-*iso*-$HC_9H_7N^+$ (Tables S2−S4, ESI†).

Considering the observed chemical behavior, thermodynamic stability, the satisfactory agreement of vibrational wavenumber and relative IR intensity between lines in group A^+ and those predicted for the N-protonated isoquinoline, and the absence of some unique features characteristic for C-protonated isoquinolines, we assign lines in group A^+ to 2-isoquinolium (*iso*-$C_9H_7NH^+$).

The observed vibrational wavenumbers are also compared with those determined with the IRMPD method[22] in Table 2. In the IRMPD spectrum, three bands were identified at 1582, 1360, and 774 cm^{-1}, which are red-shifted from corresponding lines at 1643.3 cm^{-1} (and an unobserved line predicted near 1620 cm^{-1}), 1400.1 and 1378.6 cm^{-1}, and 791.4 cm^{-1} observed in solid *p*-H_2. The red shift is presumably due to the anharmonic excitation process characteristic in the IRMPD experiments. We identified 7 lines, including the characteristic N−H stretching mode that clearly indicates the protonation site is at the N atom.

5.2 Assignments of lines in groups A and B to *iso*-C_9H_7NH and 6-*iso*-HC_9H_7N radicals

As discussed in Section 4.2, the IR lines that were induced by electron bombardment and

gained intensities during maintenance of the matrix in darkness might be due to hydrogenated isoquinoline. These lines were further classified into two groups A and B according to their behaviors on secondary photolysis at 365 nm and 405 nm. Moreover, these lines were also observed in experiments with *iso*-C_9H_7N/Cl_2/*p*-H_2 matrices irradiated with UV and IR light, in which H atoms were expected to be produced and react with *iso*-C_9H_7N to produce hydrogenated species, but not protonated species.

The experimental spectra of lines in groups A and B obtained from electron-bombarded experiment in regions 3600–2400 and 1800–600 cm^{-1} are compared with IR stick spectra of all 10 isomers of mono-hydrogenated isoquinoline radicals, simulated according to the scaled harmonic vibrational wavenumbers and IR intensities predicted with the B3LYP/6-311++G(d,p) method in Figs. S12 and S13, ESI†. The difference spectrum after secondary photolysis at 365 nm, Fig. 2c, is inverted and presented in the bottom trace of Figs. S12a and S13a, ESI†; that after secondary photolysis at 405 nm, Fig. 2d, is presented in the top trace. Lines in groups A and B are indicated with blue and red labels and arrows, respectively. Alternatively, lines in groups A and B were also observed in the UV/IR-irradiated *iso*-C_9H_7N/Cl_2/*p*-H_2 matrix. Because of an improved ratio of signal to noise and less interference, we discuss the assignments using the results of the UV/IR-irradiated *iso*-C_9H_7N/Cl_2/*p*-H_2 matrix, presented as the difference spectrum after irradiation at 420 nm from the experiments on *iso*-C_9H_7N/Cl_2/*p*-H_2, inverted Fig. 3e, in Fig. 5a to compare with predicted IR stick spectra of possible candidates *iso*-C_9H_7NH, 6-, 1-, 3-, and 4-*iso*-HC_9H_7N in Figs. 5b−5f, respectively; corresponding comparison with 5-, 7-, 8-, 4a-, and 8a-*iso*-HC_9H_7N are presented in Fig. S14, ESI†.

Assignment of lines in group A to the *iso*-C_9H_7NH radical is described as follows. In the spectral region presented in Fig. 5, intense lines in group A were observed at 1613.9, 1476.6,

1440.5, 1180.9, 988.3, 763.1, and 737.3 cm^{-1}, in satisfactory agreement with the predicted spectrum of *iso*-C_9H_7NH, which has intense lines at 1614 (ν_9, ring stretch), 1478 (ν_{13}, C=N stretch), 1440 (ν_{14}, ring stretch), 1181 (ν_{21}, ring breath + in-plane CH bend), 982 (ν_{26}, N-containing ring breath), 761, and 735 cm^{-1} (ν_{38} and ν_{39}, both out-of-plane CH bend), shown in Fig. 5b and Fig. S14, ESI†. Weaker lines of group A, which have intensities > 6 % that of the most intense line at 988.3 cm^{-1}, were observed at 1574.4, 1490.2, 1420.7, 1115.3, 1022.0, 939.2, and 577.2 cm^{-1}; these lines are near those predicted at 1577, 1489, 1411 (ν_{10}, ν_{12}, and, ν_{15}, all ring stretch), 1115 (ν_{24}, in-plane CH bend), 1026 (ν_{25}, ring breath), 932 (ν_{27}, ring deform), and 571 (ν_{42}, out-of-plane ring deform) cm^{-1}. The *iso*-C_9H_7NH isomer has a characteristic N–H stretching mode (ν_1), which is predicted to be 3518 cm^{-1} (scaled harmonic) or 3476 cm^{-1} (anharmonic); two intense lines at 3495.2 and 3491.0 cm^{-1} were observed, similar to the predicted wavenumber; matrix-site effect due to varied interactions of *iso*-C_9H_7NH with H_2 could be the reason for this observed doublet.

The simulated spectra for other isomers of isoquinolinyl radicals hydrogenated at the carbon site cannot reproduce satisfactorily the spectrum in group A (Figs. 5 and S12−S14, ESI†). As summarized in Table 4, in which all modes with calculated IR intensity greater than 10 km mol^{-1} are listed, we identified 15 modes of *iso*-C_9H_7NH. All listed modes except four CH-stretching modes have been observed. The mean absolute deviation between observed and scaled harmonic vibrational wavenumbers is 4.2 ± 4.8 cm^{-1} and that between observed and anharmonic vibrational wavenumbers is 7.9 ± 6.9 cm^{-1}, indicating a satisfactory agreement between experimental and predicted vibrational wavenumbers of *iso*-C_9H_7NH.

Assignment of lines in group B to the 6-*iso*-HC_9H_7N radical is discussed as follows. In the spectral region below 1650 cm^{-1}, intense lines in group B were observed at 1557.5, 1446.8, 1284.5, 921.1, 890.9, 810.2, 697.0, and 688.8 cm^{-1}, in satisfactory agreement with lines of 6-*iso*-HC_9H_7N

predicted at 1560, 1450, and 1282 (ν_9, ν_{11}, and ν_{17}, respectively, all ring stretch), 920 (ν_{37}, out-of-plane CH bend), 884 (ν_{26}, ring deform), 812, 698, and 686 cm^{-1} (ν_{39}, ν_{41}, and ν_{42}, respectively, all out-of-plane CH bend). Weaker lines, which have intensities <25 % that of the most intense line at 810.2 cm^{-1}, were observed at 1334.1 and 1184.4 cm^{-1}; these lines are near the lines of 6-*iso*-HC_9H_7N predicted at 1337 (ν_{16}, CH_2 wag) and 1185 (ν_{20}, ring stretch) cm^{-1}, respectively. Another weaker line, observed at 1041.5 cm^{-1} and predicted at 1048 cm^{-1} for the ring breathing (ν_{23}) mode, is tentatively assigned to 6-*iso*-HC_9H_7N because the line was only observed in the electron-gun experiment.

In the CH-stretching region, relatively intense lines were observed at 3059.0, 3045.1, 3025.3 in experiments with *iso*-C_9H_7N/Cl_2/*p*-H_2 (Fig. 5a), but definitive mode assignments of these lines were difficult, partly because of severe interference from intense absorptions lines of the parent and partly because of anharmonic interactions. Two lines at 2826.4, and 2802.5 cm^{-1} (Figs. S12 and S13) were observed in electron bombardment experiments; they were assigned to the characteristic symmetric and antisymmetric CH_2-stretching (ν_7 and ν_{33}) modes of 6-*iso*-HC_9H_7N. These two lines could not be definitively identified in experiments with *iso*-C_9H_7N/Cl_2/*p*-H_2 (Fig. 5a) because they were interfered with by the intense absorption of HCl and its complexes.

The simulated spectra for other isomers of isoquinolinyl radicals, *iso*-C_9H_7NH, 1-, 3-, 4-, 5-, 7-, 8-, 4a-, and 8a-*iso*-HC_9H_7N, cannot reproduce satisfactorily the wavenumbers and relative intensities of lines in group B (Figs. 5 and S12 to S14, ESI†). As listed in Table 4 for lines, we assigned 16 lines in group B to 6-*iso*-HC_9H_7N. All listed modes with IR intensity greater than 10 km mol^{-1} except two CH-stretching modes and a line predicted near 1419 cm^{-1} (ν_{13}) have been observed; the latter line was predicted to have IR intensity of only 1 km mol^{-1} with the anharmonic calculations. The mean absolute deviation between observed and scaled harmonic vibrational

wavenumbers is 6.5 ± 8.3 cm^{-1} and that between observed and anharmonic vibrational wavenumbers is 9.1 ± 9.5 cm^{-1}, indicating a satisfactory agreement between experimental and predicted wavenumbers.

5.3 Assignments of lines in groups C and D to 7-*iso*-HC_9H_7N and 8-*iso*-HC_9H_7N radicals

Intensities of lines in group C decreased upon irradiation at 553, 540, 420, and 405 nm and remained unchanged upon irradiation at 360 nm; in contrast, intensities of lines in group D increased upon irradiation at 553, 420, and 405 nm, decreased upon irradiation at 360 nm, and remained unaltered upon irradiation at 540 nm (Table 3). The difference spectrum in Fig. 3b, recorded after UV/IR irradiation of the *iso*-C_9H_7N/Cl_2/*p*-H_2 matrix, was reproduced in the lower trace of Fig. 6a after truncating negative lines, and the difference spectrum upon secondary irradiation of the matrix at 553 nm, Fig. 3c, was reproduced in the upper trace of Fig. 6a; for clarity, only the region 1000−600 cm^{-1} is shown. Lines in groups C and D are marked with green and brown labels and arrows, respectively. The stick spectra of isomers of 7- and 8-*iso*-HC_9H_7N radicals simulated according to scaled harmonic vibrational wavenumbers and IR intensities are depicted in Figs. 6b and 6c, respectively, and compared with the observed lines in groups C and D. Figure S15, ESI†, compares lines in groups C and D with all 10 isomers of isoquinolinyl radical in region 1700−1000 cm^{-1}; those in regions 3600−3450 and 3100−2700 cm^{-1} are shown in Fig. S16, ESI†.

As shown in these figures, the spectral pattern of observed lines in group C agrees satisfactorily with IR stick spectrum of the 7-isoquinolinyl radical, 7-*iso*-HC_9H_7N, but disagree with IR stick spectra of other mono-hydrogenated radicals. Table 4 compares the observed wavenumber and relative IR intensities of lines in group C with both scaled harmonic and anharmonic vibrational wavenumbers and relative IR intensities predicted for 7-*iso*-HC_9H_7N.

Intense lines observed at 1551.2, 1331.5, 1284.3, 892.0, 908.4, 817.5, and 682.2 cm^{-1} agree with those predicted at 1553 (ν_9, ring stretch), 1334 (ν_{16}, CH_2 wag coupled with ring stretch), 1286 (ν_{17}, ring stretch), 883 (ν_{26}, C6C7C8 symmetric stretch), 912 (ν_{37}, CH_2 rock), 821 (ν_{39}, out-of-plane CH bend), and 681 (ν_{42}, out-of-plane C5H bend) cm^{-1}. Other weak lines with intensity <12 % of the most intense line at 817.5 cm^{-1} were observed at 1617.2, 1205.1, 1017.9, 935.4(?), 907.6, and 720.9(?) cm^{-1}; two lines were marked with question marks because they were not clearly visible after IR irradiation, likely due to small intensity. These lines agree with predicted vibrational wavenumbers at 1641 (ν_8, ring stretch), 1208 (ν_{20}, in-plane CH bend), 1016 (ν_{24}, ring stretch), 935 (ν_{36}, out-of-plane CH bend), 914 (ν_{25}, ring deform), and 694 (ν_{41}, 715 from anharmonic calculations, out-of-plane CH bend) cm^{-1}.

In the CH-stretching region, lines at 3057.8 and 3025.6 cm^{-1} in group C agree with predicted vibrational wavenumbers at 3065/3059 (3046/3044, ν_2/ν_3) and 3028 (3000, ν_6) cm^{-1}; values in parentheses are anharmonic vibrational wavenumbers. Lines in the region 2910–2790 cm^{-1} corresponding to symmetric and antisymmetric CH_2 stretching modes cannot be assigned definitively because of severe interference of HCl and its complexes. Table 4 lists all vibrational modes with IR intensity greater than 10 km mol^{-1}. A total of 15 lines in group C were assigned to 7-*iso*-HC_9H_7N (Table 4). All listed modes (with harmonic IR intensity >10 km mol^{-1}) except two CH-stretching mode and a line predicted near 1435 cm^{-1} have been observed; the latter line was predicted to have IR intensity of only 3 km mol^{-1} in anharmonic calculations. The average absolute deviation between observed and scaled harmonic (anharmonic) vibrational wavenumbers is 3.2 ± 2.3 (9.8 ± 7.3) cm^{-1}, indicating a satisfactory agreement between experimental and predicted wavenumbers.

Similarly, lines in group D can be assigned to the 8-isoquinolinyl radical, 8-*iso*-HC_9H_7N.

The five most intense lines observed at 1576.2, 1467.6, 1432.2, 830.5, and 653.7 cm^{-1} are predicted at 1585 (ν_8, ring stretch), 1472 (ν_{11}, ring stretch), 1431 (ν_{12}, CH_2 wag coupled with ring stretch), 834, and 654 cm^{-1} (ν_{39} and ν_{42}, both out-of-plane CH bend), respectively. Additional two weak lines were observed at 1245.5 and 941.6 cm^{-1}, near scaled harmonic vibrational wavenumber predicted at 1259 (ν_{18}, ring deform) and 935 (ν_{25}, ring deform) cm^{-1}, respectively. The simulated spectra for other isomers of isoquinolinyl radicals cannot reproduce the wavenumbers and relative intensities of lines in group D (Figs. S15 and S16, ESI†).

Moreover, two lines at 3083.9 and 3076.6 cm^{-1} in the CH-stretching region agree with the predicted vibrational wavenumbers of ν_1 and ν_2 modes at 3080 (3092) and 3070 (3062) cm^{-1}; values in parentheses are anharmonic vibrational wavenumbers (Fig. S16, ESI†). However, lines in region 2910–2790 cm^{-1} cannot be assigned definitively because of interference from HCl and its complexes. Table 5 compares the observed wavenumber and relative IR intensities for 9 lines in group D with both scaled harmonic and anharmonic vibrational wavenumbers and relative IR intensities predicted for 8-*iso*-HC_9H_7N. All listed modes (with calculated IR intensity greater than 10 km mol^{-1}) have been observed except four CH-stretching modes. The average absolute deviation between observed and scaled harmonic (anharmonic) vibrational wavenumbers is 4.8 ± 3.8 (6.5 ± 3.3) cm^{-1}.

5.4 Assignments of lines in groups E and F to 4-*iso*-HC_9H_7N and 5-*iso*-HC_9H_7N radicals

Intensities of lines in group E decreased upon secondary photolysis at 540, 420, and 360 nm and remained unchanged on photolysis at 553 and 405 nm; in contrast, intensities of lines in group F increased upon secondary photolysis at 420 and 405 nm, but decreased upon photolysis at 360 nm, and remained unaltered on photolysis at 553 and 540 nm. The difference spectrum in Fig. 3b, recorded after UV/IR irradiation of the matrix, was reproduced in the lower trace of Fig. 6d for the

region 1000−600 cm^{-1} after truncating negative lines, whereas the difference spectrum upon secondary irradiation at 420 nm, Fig. 3e, was reproduced in the upper trace of Fig. 6d. Lines in groups E and F are indicated with light blue and purple labels and arrows, respectively. Figs. 6e and 6f depict IR stick spectra of 4- and 5-*iso*-HC_9H_7N according to predicted scaled vibrational harmonic wavenumbers and IR intensities. Observed lines in groups E and F are compared with the IR stick spectra of all 10 isomers of mono-hydrogenated quinoline in regions 1700−1000 and 3600−3450 and 3100−2700cm^{-1} in Figs. S17 and S18, ESI†, respectively.

The spectral pattern of observed lines in group E agrees satisfactorily with the IR stick spectrum of 4-isoquinolinyl radical, 4-*iso*-HC_9H_7N, but disagrees with predicted spectra of other mono-hydrogenated radicals. Table 5 compares the observed wavenumber and relative IR intensities with both scaled harmonic and anharmonic vibrational wavenumbers and relative IR intensities predicted for 4-*iso*-HC_9H_7N. The two most intense lines observed at 1245.9 and 748.1 cm^{-1} are predicted at 1249 (ν_{18}, ring stretch) and 746 (ν_{40}, out-of-plane CH bend). Two weak lines were observed at 1483.7 and 1269.4 cm^{-1}, near scaled harmonic wavenumber predicted at 1485 (ν_{11}, ring stretch) and 1274 (ν_{17}, ring stretch) cm^{-1}. In the CH-stretching region, one line observed at 3087.9 cm^{-1} agrees with the predicted scaled harmonic vibrational wavenumber at 3083 cm^{-1} (ν_1) or the anharmonic vibrational wavenumber 3068 cm^{-1} (ν_2), as shown in Fig. S18, ESI†. This line is tentatively assigned to ν_1 of 4-*iso*-HC_9H_7N, but identification of other intense lines 3070 (3068, ν_2), 3026 (3012, ν_6), and 2874 (2832, ν_7) cm^{-1} with IR intensities 21, 25, and 29 km mol^{-1}, respectively, are difficult because of the severe interference with the parent or products. These five lines in group E are hence assigned to 4-*iso*-HC_9H_7N. All lines predicted to have IR intensity greater than 10 km mol^{-1} except four have been observed. However, the missing lines predicted near 1511 and 782 cm^{-1} have intensities 5 and 2 km mol^{-1} in anharmonic calculations. Two

additional lines predicted at 782 and 1417 cm^{-1} (ν_{39} and ν_{13}) with IR intensities 21 and 11 km mol^{-1}, respectively, could not be positively identified because of the interference with the parent and with 6-*iso*-HC_9H_7N, respectively. The average absolute deviation between observed and scaled harmonic (anharmonic) vibrational wavenumbers is 2.8 ± 1.2 (3.6 ± 3.2) cm^{-1}.

Observed lines in group F agree satisfactorily with IR stick spectrum of 5-isoquinolinyl radical, 5-*iso*-HC_9H_7N, but disagree with those of other mono-hydrogenated radicals. Table 5 compares the observed wavenumber and relative IR intensities predicted for 5-*iso*-HC_9H_7N. Three most intense lines observed at 821.9, 708.6, and 652.3 cm^{-1} are predicted at 823 (ν_{39}, out-of-plane CH bend), 710 (ν_{41}, out-of-plane ring deform), and 651 cm^{-1} (ν_{42}, out-of-plane CH bend). Two additional lines were observed at 1402.0 and 1201.3 cm^{-1}, near scaled harmonic vibrational wavenumber predicted at 1418 (ν_{13}, CH_2 scissor) and 1202 (ν_{20}, CH_2 wag coupled with ring stretch). Only two lines of 5-*iso*-HC_9H_7N with predicted IR intensities greater than 10 km mol^{-1} in the region 1700–600 cm^{-1}, 1582 (ν_8, 18 km mol^{-1}) and 1426 cm^{-1} (ν_{12}, 10 km mol^{-1}) remain unobserved because of interference; the former might be interfered with by the line of group A at 1574.4 cm^{-1} and the latter one has intensity of 5 km mol^{-1} according to anharmonic calculations. In the CH-stretching region, one line observed at 3083.2 cm^{-1} agrees with the predicted scaled harmonic (anharmonic) vibrational wavenumbers at 3080 (3082, ν_1) cm^{-1}, as shown in Fig. S18, ESI†. This line is tentatively assigned to the ν_1 mode of 5-*iso*-HC_9H_7N, but identification of other intense lines 3070 (3054, ν_2), 3064 (3038, ν_3), 3031 (2995, ν_6), and 2874 (2841, ν_7) cm^{-1} is difficult because of the severe interference of parent or products in the CH-stretching region. These six lines in group F are hence assigned to 5-*iso*-HC_9H_7N; the average absolute deviation between observed and scaled harmonic (anharmonic) vibrational wavenumbers is 4.1 ± 5.9 (2.3 ± 2.1) cm^{-1}.

5.5 Assignments of lines in group G and H to 1-*iso*-HC_9H_7N and 3-*iso*-HC_9H_7N radicals

Apart from those lines assigned to groups A–E, we observed four lines in group G with intensities that increased upon secondary irradiation at 405 nm, decreased upon secondary irradiation at 360 nm, and remained unchanged on irradiation at 553, 540, and 420 nm. We also observed two weak lines with intensities decreased upon secondary irradiation at 553 and 405 nm and remained unaltered upon irradiation at other wavelengths; these lines are categorized as group H. The difference spectrum in Fig. 3c, recorded after UV/IR irradiation of the matrix, was reproduced in the lower trace of Fig. 6g after truncating negative lines; the difference spectrum recorded upon secondary irradiation of the matrix at 360 nm, Fig. 3g, was reproduced in the upper trace of Fig. 6g for region 1000−600 cm^{-1}. Lines in groups G and H are denoted with orange and olive labels and arrows, respectively. Figures 6h and 6i depict IR stick spectra of 1- and 3-*iso*-HC_9H_7N, simulated according to scaled vibrational harmonic wavenumbers, for comparison with observed lines. Observed lines in groups G and H in region 1700−1000 cm^{-1} are compared with the IR stick spectra of all 10 isomers of mono-hydrogenated quinoline, as illustrated in Fig. S19, ESI†.

Even though only four lines were observed in group G, they correspond well with lines of 1-*iso*-HC_9H_7N with predicted IR intensities greater than 10 km mol^{-1} in region 1700–600 cm^{-1} except two lines predicted at 945 and 699 cm^{-1} (ν_{25} and ν_{42} with IR intensity 10 and 15 km mol^{-1}, respectively); the absence of these two lines is due to interference from the parent and 6-*iso*-HC_9H_7N (group B), respectively. Table 6 compares the observed wavenumber and relative IR intensities with both scaled harmonic and anharmonic vibrational wavenumbers and relative IR intensities predicted for 1-*iso*-HC_9H_7N. The four lines observed at 1416.6, 918.3, 769.2 and 714.6 cm^{-1} were predicted at 1414 (ν_{13}, CH_2 scissor coupled with in-plane C3H bend), 920 (ν_{26}, ring deform), 772 and 715 cm^{-1} (ν_{40} and ν_{41}, both out-of-plane CH bend). Similarly, the CH-stretching

region could not be characterized because of severe interference from the parent and products. Even though only a limited number of lines were observed, we feel confident to assign these lines in group G to 1-*iso*-HC_9H_7N because major lines were observed. The average absolute deviation between observed and scaled harmonic (anharmonic) vibrational wavenumbers is 2.6 ± 1.9 (9.6 ± 7.1) cm^{-1}.

Two lines in group H observed at 1642.7 and 876.4 cm^{-1}, similar to those predicted at 1644 (ν_8, CN stretch coupled with CH_2 scissor) and 870 (ν_{26}, ring stretch) cm^{-1}, which are the second and third most intense lines of 3-*iso*-HC_9H_7N in region 1700−600 cm^{-1}. However, definitive identification of the most intense line predicted at 746 cm^{-1} was unachievable because of interference from the parent and the most intense line in group E (4-*iso*-HC_9H_7N) at 748.1 cm^{-1}. The four other missing lines in region 600−1700 cm^{-1} were predicted to have IR intensities less than 14 km mol^{-1}, and all of them were predicted to have IR intensities less than 9 km mol^{-1} with the anharmonic calculations. The comparison of observed wavenumbers and those predicted for 3-*iso*-HC_9H_7N is listed in Table 6. Because only two lines were observed, we hence tentatively assigned the observed two lines in group H to 3-*iso*-HC_9H_7N. The smallest number of observed lines is consistent with the estimated smallest mixing ratio, 0.42 ± 0.01 ppm, among all observed isomers.

5.6 Mechanism of formation in *p*-H_2

The mechanism to form 2-isoquinolinium (*iso*-$C_9H_7NH^+$) is expected to be similar to those for the formation of 1-quinolinium cation[25] and protonated cyclic compounds including PAH.[22, 23] During deposition of *p*-H_2 under electron bombardment, H_2 molecules are ionized by electron to produce H_2^+; the H_2^+ product readily react with another H_2 molecule to produce H and H_3^+. Because the proton affinity of isoquinoline, 957 kJ mol^{-1} for the formation of *iso*-$C_9H_7NH^+$ and

>689 kJ mol^{-1} for the formation of *iso*-$H^+C_9H_7N$, is much greater than that of H_2, 422 kJ mol^{-1},[20] proton transfer from H_3^+ to isoquinoline occurs readily. The exothermicity of the proton transfer reaction, H_3^+ + *iso*-$C_9H_7N \rightarrow H_2$ + *iso*-$C_9H_8N^+$, is significantly greater than the energy barriers for proton transfer between isomers of *iso*-$C_9H_8N^+$ (Fig. S2, ESI†); all isomers can be produced, in principle, via the proton transfer reaction. However, the observation of only *iso*-$C_9H_7NH^+$ in our experiments indicates that either the proton transfer to the N site of isoquinoline is significantly more favorable or the energy dissipation by solid *p*-H_2 is efficient enough to quench the isomerization process, so that only the thermodynamically most stable *iso*-$C_9H_7NH^+$ was produced. Moreover, no fragmentation or ring-opening products of *iso*-$C_9H_8N^+$ could be identified in these experiments. Hansen et al. reported the significant formation of HCN in their UV photodissociation experiments of protonated quinoline and isoquinoline,[41] but we did not observe HCN (expected to be near 3303 and 720 cm^{-1})[42] either. These authors calculated an energy threshold of ~448 kJ mol^{-1} for the formation of HCN and ring-opening coproducts. Even though this energy is smaller than the exothermicity of H_3^+ + *iso*-$C_9H_7NH \rightarrow$ *iso*-$C_9H_7NH^+ + H_2$, ~534 kJ mol^{-1}, one would expect the excess energy of *iso*-$C_9H_7NH^+$ be rapidly dissipated in solid *p*-H_2 below its dissociation threshold.

In electron bombardment experiments, the isoquinolinyl radicals are expected to be formed on neutralization of isoquinolinium cation, *iso*-$C_9H_8N^+ + e^- \rightarrow$ *iso*-C_9H_8N, or by the reaction of *iso*-C_9H_7N with an H atom, H + *iso*-$C_9H_7N \rightarrow$ *iso*-C_9H_8N. The former process tends to produce the neutral counterpart of protonated species; therefore, the formation of *iso*-C_9H_7NH is expected, which is in accordance with our experiments that lines in group A (assigned to *iso*-C_9H_7NH) were observed. The mixing ratios of *iso*-$C_9H_7NH^+$ and *iso*-C_9H_7NH after electron-bombarded matrix deposition were estimated to be 0.65 ± 0.09 and 2.2 ± 1.1 ppm, respectively, in which errors

represent the standard deviations in averaging mixing ratios derived from several line. After maintenance of the matrix in darkness for 10 h, the mixing ratio of *iso*-$C_9H_7NH^+$ decreased by 0.25 ± 0.16 ppm and that of *iso*-C_9H_7NH increased by 0.9 ± 0.5 ppm, indicating that the observed abundance of *iso*-C_9H_7NH might not be explained by considering the neutralization process alone. However, because of the large errors that might be associated with the predicted IR intensities, we cannot exclude the possibility that the mixing ratio of *iso*-C_9H_7NH was overestimated as compared with that of *iso*-$C_9H_7NH^+$. In the electron-bombardment experiments, for hydrogenated species, in addition to *iso*-C_9H_7NH, we were able to identify clearly only the formation of 6-*iso*-HC_9H_7N radical (lines in group B). The mixing ratio of 6-*iso*-HC_9H_7N after the matrix deposition was estimated to be 0.9 ± 0.3 ppm and its increase after maintenance of the matrix in darkness for 10 h is 1.0 ± 0.4 ppm, similar to the increase of *iso*-C_9H_7NH (0.9 ± 0.5 ppm). It is unclear why only 6-*iso*-HC_9H_7N among all possible carbon sites for hydrogenation was observed.

For H-addition reactions, because they have barriers > 20 kJ mol^{-1}, quantum tunneling is required in low-temperature solid *p*-H_2. The probability of tunneling reaction depends on the width and height of the barrier. The barrier height for the formation of isoquinolinyl radicals are predicted to be 21–27 kJ mol^{-1} for *iso*-C_9H_7NH and 1-, 3-, 4-, 5-, 6-, 7-, 8-*iso*-HC_9H_7N, respectively, but much greater (~50 kJ mol^{-1}) for 4a- and 8a-*iso*-HC_9H_7N. It is hence conceivable that all isomers of *iso*-C_9H_8N except 4a- and 8a-*iso*-HC_9H_7N can be produced from the reaction of H with isoquinoline.

In the H-atom reactions, 8 isomers of *iso*-C_9H_8N were observed; the estimated mixing ratios for *iso*-C_9H_7NH, 1-, 3-, 4-, 5-, 6-, 7-, and 8-*iso*-HC_9H_7N are 2.8 ± 0.5, 1.5 ± 0.3, 0.42 ± 0.01, 2.5 ± 0.3, 1.5 ± 0.3, 2.1 ± 1.2, 1.1 ± 0.4, and 1.6 ± 0.1 ppm, respectively. Because of errors in the calculated IR intensities and barriers of hydrogenation reactions, obtaining a definitive relationship

between observed mixing ratios and reaction barriers is difficult. The rate of tunneling reactions depends on the barrier height and the width of the barrier, which requires more sophisticated quantum-chemical calculations. No apparent correlation between observed mixing ratios and barriers for formation calculated with the CCSD(T) method could be derived. Nevertheless, if one compares the barriers calculated with the B3LYP method, formation of *iso*-C_9H_7NH is associated with a significantly smaller barrier (~6 kJ mol^{-1} vs. >11 kJ mol^{-1}) and the largest mixing ratio (2.8 ± 0.5 ppm) for *iso*-C_9H_7NH; formation of 3-*iso*-HC_9H_7N is associated with the largest barrier (15 kJ mol^{-1} from B3LYP and 27 kJ mol^{-1} from CCSD(T)) and the smallest mixing ratio (0.42 ± 0.01 ppm).

5.7 Secondary irradiation

The UV spectra of *iso*-C_9H_7N and all 10 mono-hydrogenated isomers of *iso*-C_9H_7N predicted with the TD-B3LYP/6-311++G(d,p) method are depicted in Fig. S20, ESI†; associated wavelengths and oscillator strengths are listed in Tables S11−S13, ESI†. The calculated UV spectra provide satisfactory predictions in the choice of wavelengths used for secondary irradiation. The wavelengths for secondary irradiation were selected to be greater than 300 nm to avoid photolysis of the parent, which was predicted to have UV absorption starting near 300 nm. The significant destruction of 7-*iso*-HC_9H_7N and 3-*iso*-HC_9H_7N upon photolysis at 553 nm agrees well with the predicted absorption bands near 544 and 520 nm, corresponding to HOMO → LUMO transition for both isomers. The increase of 8-*iso*-HC_9H_7N at this wavelength seems to indicate that 7-*iso*-HC_9H_7N → 8-*iso*-HC_9H_7N isomerization occurs. We could hence differentiate these three mono-hydrogenated isomers of *iso*-C_9H_7N upon irradiation at 553 nm. At 420 and 405 nm, 1-, 5- and 8-*iso*-HC_9H_7N either increase in intensity or remained nearly the same; these three isomers are the ones that have no significant absorption for wavelength greater than 320 nm; the increase might

be due to the hydrogen transfer from a neighboring site. For 3-*iso*-HC_9H_7N, it has no significant absorption for wavelength greater than 370 nm, so we observed no change at 420 nm and a small decrease at 405 nm. The destruction of 1-, 4-, 5-, and 8-*iso*-HC_9H_7N upon irradiation at 360 nm is consistent with the predicted absorption bands at 322/347, 324/342, 330, and 322/348 nm, respectively, with oscillator strength greater than 0.11. The destruction of *iso*-C_9H_7NH upon irradiation at 540, 420, and 405 nm agrees with the predicted absorption bands near 585/483 and 426 nm.

5.8 Implication to astrochemistry

The UIR emission spectrum observed from the Orion Bar PDR[43] is compared with the stick IR spectra of protonated isoquinoline, protonated quinoline,[25] and protonated naphthalene (1-$C_{10}H_9^+$)[27] in Fig. S21, ESI†. In the region ~6.2 μm, the line of 1-$C_{10}H_9^+$ in solid *p*-H_2 at 1618.7 cm^{-1} (~6.18 μm) is blue-shifted to 1643.3 cm^{-1} (ν_9, ~6.09 μm) in protonated isoquinoline and to 1641.4 cm^{-1} (~6.09 μm) in protonated quinoline. The line of *iso*-C_9H_7NH in solid *p*-H_2 at 1554.7 cm^{-1} (ν_{12}) is also blue-shifted from that of 1-$C_{10}H_9^+$ at 1510 cm^{-1}. Two additional lines of 1-$C_{10}H_9^+$ in solid *p*-H_2 were observed at 1556.7 and 1580.8 cm^{-1}, the corresponding lines of *iso*-C_9H_7NH were predicted at 1587 and 1620 cm^{-1}, but was not observed due to interference. Because we recorded absorption spectra, which should be slightly different from the UIR emission spectra. Typically, the maxima of emission bands are slightly red-shifted from those of absorption bands because of the anharmonicity associated with the vibrationally excited emitting states produced on UV irradiation.[14,44] Thus, the band associated with ring stretching modes of protonated quinoline and isoquinoline match the 6.2-μm UIR band better than those of protonated naphthalene. Relatively intense lines of the out-of-plane CH-bending mode were observed at 791.4 cm^{-1} (12.64 μm) in protonated isoquinoline and at 790.2 cm^{-1} (12.65 μm) in protonated quinoline, matching

the 12.8-μm band of UIR emission, although the UIR bands in region 12.4–13.3 μm are generally considered to originate from out-of-plane C–H bending modes associated with trio CH that has three adjacent peripheral CH moieties.[45,46,47] The other UIR bands near 7.7, 8.6, and 11.2 μm are unobserved or weak in the absorption spectra of protonated quinoline and protonated isoquinoline; these two protonated species are hence unlikely to be the carrier of the UIR bands. This is consistent with the expectation that quinoline and isoquinoline are too small to survive the intense UV field in interstellar media. Therefore, it is desirable to extend the current investigation to larger H^+PANH to confirm that the blue shifts of ring stretching modes and the appearance of the band ~12.7 μm are common in H^+PANH.

6. Conclusion

Electron bombardment during matrix deposition of a mixture of isoquinoline (*iso*-C_9H_7N) and *p*-H_2 produced *iso*-$C_9H_7NH^+$, *iso*-C_9H_7NH, and 6-*iso*-HC_9H_7N; their IR lines were classified according to their behavior after maintenance of the matrix in darkness for prolonged time and upon secondary photolysis at 365 and 405 nm. To enhance the hydrogenation reactions, we irradiated an *iso*-C_9H_7N/Cl_2/*p*-H_2 matrix at 365 nm, followed by IR light to generate H atoms for the reaction with *iso*-C_9H_7N; the formation of all 8 isomers of *iso*-C_9H_8N radicals singly hydrogenated on non-ring-sharing atoms were observed, indicating the Cl-induced hydrogenation reaction is more effective than electron bombardment for hydrogenation. The IR lines observed in Cl_2-doped experiments were classified into eight groups and assigned to *iso*-C_9H_7NH, 6-, 7-, 8-, 4-, 5-, 1-, and 3-*iso*-HC_9H_7N according to their behavior upon secondary photolysis at 553, 540, 420, 405, and 360 nm and comparison with quantum-chemical calculations at the B3LYP/6-311++G(d,p) level of theory. Nearly all lines predicted to have IR intensities greater than 10 km mol^{-1} have been observed for *iso*-C_9H_7NH, 6-, 7-, 8-, 4-, and 5-*iso*-HC_9H_7N; assignment of lines

in group H to 3-*iso*-HC_9H_7N is tentative, because only two lines were unambiguously assigned.

Three bands of gaseous *iso*-$C_9H_7NH^+$ were observed previously with the IRMPD method.[22] In addition to these three features, we observed additional 4 lines of *iso*-$C_9H_7NH^+$ to provide improved IR characterization of this species. The IR spectra of all isomers of mono-hydrogenated isoquinoline are previously unreported; they provide important information for future identification of these species in combustion or astronomical environments. Observation of all 8 isomers of the feasible mono-hydrogenated PAH in a single experiment has never been demonstrated previously; the high efficiency of H-tunneling reaction, absence of multiple hydrogenation, and simplified spectra with narrow lines in matrix isolation are unique characters of this type of H reactions in solid *p*-H_2 using Cl atoms and IR light to induce hydrogenation reactions and allow identification of various isomers.

Lines of protonated naphthalene (1-$C_{10}H_9^+$) at 1618.7,1580.8/1556.7, and 1510.0 cm^{-1} (Ref. 27) are blue-shifted to 1641.4, 1598.4, and 1562.0 cm^{-1} in protonated quinoline, $C_9H_7NH^+$,[25] and 1643.3, (~1620/1587), and 1554.7 cm^{-1} in protonated isoquinoline, *iso*-$C_9H_7NH^+$; the predicted lines at 1620/1587 cm^{-1} were unobserved because of interference. $C_9H_7NH^+$ and *iso*-$C_9H_7NH^+$ are not expected to be candidates for the carrier of the UIR band because they are unlikely to survive the strong UV field in the interstellar media, considering the small sizes. Nevertheless, this observation experimentally supports the proposed blue shift of the ring stretching bands upon substitution of a CH moiety of H^+PAH with a nitrogen atom to form H^+PANH; these blue-shifted band matches the UIR bands near 6.2 μm better than those of H^+PAH.

Supplementary information

Electronic supplementary information (ESI) available: Tables: scaled harmonic and anharmonic vibrational wavenumbers and IR intensities of 10 isomers of isoquinolinium cation and 10 isomers

of isoquinolinyl radical. Comparison of observed vibrational wavenumbers of isoquinoline with calculated values. Estimated mixing ratios of isoquinolinyl radical. Vertical excitation wavelengths and oscillator strengths of all isomers of isoquinolinyl radicals. Figures: calculated geometries and relative energies of isomers of isoquinolinium cations and isoquinolinyl radicals. Potential energy diagrams for various isomers of isoquinolinium cations and transition states for isomerization and for various isomers of isoquinolinyl radicals and transition states for their formation and isomerization. Predicted IR spectra for 10 isomers of isoquinolinium cations and isoquinolinyl radicals. Comparison of experimental and predicted IR spectra of *iso*-C_9H_7N. Calibration curve for observed and calculated harmonic vibrational wavenumbers of *iso*-C_9H_7N. Spectra of *iso*-$C_9H_7N/Cl_2/p$-H_2 matrices at various stages of experiments. Comparison of experimental spectrum of group A^+ with simulated spectra of 10 isomers of isoquinolinium cations. Comparison of experimental spectra of groups A and B, groups C and D, groups E and F, and groups G and H with simulated spectra of 10 isomers of isoquinolinyl radicals. Predicted UV spectra of isomers of hydrogenated isoquinoline. Comparison of experimental spectra of protonated isoquinoline, isoquinoline, and naphthalene with UIR bands observed from Orion Bar PDR. See https://doi.org/10.1039/d2cpxxxxxxx.

Conflict of interest

There are no conflicts to declare.

Acknowledgments

This work was supported by Ministry of Science and Technology, Taiwan (grants MOST110-2639-M-A49-001-ASP and MOST110-2634-F-009-026) and Center for Emergent Functional Matter

Science of National Chiao Tung University from The Featured Areas Research Center Program within the framework of the Higher Education Sprout Project by the Ministry of Education (MOE) in Taiwan. Japan Society for the Promotion of Science (JSPS KAKENHI grant Nos. JP18K03717 and JP21H01139) partially supported this work.

Table 1 Relative energies of isomers of protonated isoquinoline and relative energies and barrier heights for the formation of various isomers of mono-hydrogenated isoquinoline from hydrogenation of isoquinoline calculated with the CCSD(T)/6-311++G(d,p)//B3LYP/ 6-311++G(d,p) method

Site[a]	*iso*-$C_9H_8N^+$	*iso*-C_9H_8N	
	Relative energy[b] /kJ mol^{-1}	Relative energy[b] /kJ mol^{-1}	Barrier for formation[c] /kJ mol^{-1}
1	200 (198)[d]	6 (23)[d]	24 (14)[d]
2	0[e]	0[f]	23 (6)
3	190 (186)	22 (39)	27 (15)
4	169 (166)	3 (19)	22 (11)
5	171 (167)	2 (20)	21 (11)
6	209 (204)	24 (41)	26 (14)
7	183 (180)	24 (41)	26 (14)
8	190 (186)	3 (20)	22 (12)
4a	267 (271)	100 (125)	46 (39)
8a	240 (245)	91 (118)	52 (36)

[a] See Fig. 1 for protonation or hydrogenation sites. [b] Zero-point vibrational energies are corrected using unscaled harmonic vibrational wavenumbers calculated with the B3LYP/6-311++G(d,p) method. [c] Energy of the transition state relative to that of H + *iso*-C_9H_7N. [d] Energies calculated with the B3LYP//6-311++G(d,p) are listed in parentheses for comparison. [e] The energy of *iso*-$C_9H_7NH^+ + H_2$ is smaller than *iso*-$C_9H_7NH + H_3^+$ by 534 (538) kJ mol^{-1}, implying a proton affinity of 957 (989) kJ mol^{-1} for *iso*-C_9H_7N on the N-atom site. [f] The energy of *iso*-C_9H_7NH is smaller than H + *iso*-C_9H_7N by 111 (148) kJ mol^{-1}.

Table 2 Comparison of observed vibrational wavenumbers (cm^{-1}) and relative IR intensities of lines in group A^+ with scaled harmonic and anharmonic vibrational wavenumbers (cm^{-1}) and IR intensities (km mol^{-1}) of *iso*-$C_9H_7NH^+$ predicted with the B3LYP/6-311++G(d, p) method

Mode	Sym.	B3LYP/6-311++G(d, p)				Experiments		
		Scaled harmonic		Anharmonic		IRMPD[a]	*p*-H_2	
ν_1	a'	3430[b]	(208)[c]	3407	(180)[c]		3397.2	(250)[d]
ν_9	a'	1639	(83)	1625	(60)	1582	1643.3	(40)
ν_{10}	a'	1620	(27)	1610	(19)			
ν_{11}	a'	1587	(15)	1576	(11)			
ν_{12}	a'	1559	(7)	1550	(10)		1554.7	(10)
ν_{13}	a'	1500	(14)	1494	(12)		1497.3	(7)
ν_{16}	a'	1394	(43)	1382	(40)	1360	1400.1	(69)
ν_{17}	a'	1382	(49)	1378	(25)		1378.6	(31)
ν_{18}	a'	1285	(13)	1285	(12)			
ν_{40}	a''	788	(150)	806	(39)	774	791.4	(100)
ν_{42}	a''	724	(23)	715	(58)		[e]	
ν_{44}	a''	471	(29)	471	(32)			

[a] Infrared multiphoton dissociation (IRMPD) experiments by Galué *et al*.[22] [b] Harmonic vibrational wavenumbers scaled according to $0.9122\,x + 174.3$ for wavenumbers >2000 cm^{-1} and $0.9823\,x + 0.6$ for wavenumbers <2000 cm^{-1}. [c] The IR intensities in km mol^{-1} are listed in parentheses; only modes with IR intensities > 10 km mol^{-1} are listed, unless a mode was observed. [d] Percentage IR intensities with respect to that of the line at 791.4 cm^{-1} are listed in parentheses. [e] Interference by absorption of *p*-H_2.

Table 3 Summary of behaviors on secondary irradiation of various groups of lines of *iso*-C_9H_8N

Group	Assignments	553 nm	540 nm	420 nm	405 nm	360 nm
A	*iso*-C_9H_7NH	no change	decrease (~ 6 %)[b]	decrease*[a] (~ 11 %)	decrease (~ 9 %)	no change
B	6-*iso*-HC_9H_7N	no change	no change	decrease* (~ 12 %)	decrease (~ 8 %)	no change
C	7-*iso*HC_9H_7N	decrease* (~ 13 %)	decrease (~ 3 %)	decrease (~ 8 %)	decrease (~ 6 %)	no change
D	8-*iso*-C_9H_7NH	increase* (~ 15 %)	no change	increase (~ 3%)	increase (~ 1%)	decrease (~ 2 %)
E	4-*iso*-C_9H_7NH	no change	decrease* (~ 7 %)	decrease (~ 2%)	no change	decrease (~ 1 %)
F	5-*iso*-C_9H_7NH	no change	no change	increase* (~ 6%)	increase (~ 2 %)	decrease (~ 2 %)
G	1-*iso*-C_9H_7NH	no change	no change	no change	increase (~ 3 %)	decrease* (~ 5 %)
H	3-*iso*-C_9H_7NH	decrease* (~ 4 %)	no change	no change	decrease (~ 2 %)	no change

[a]The most significant variation in each species among all wavelengths is marked with *. [b]The percentage variation is based on the spectrum measured after IR irradiation.

Table 4 Comparison of observed vibrational wavenumbers (in cm^{-1}) and relative IR intensities of lines in groups A−C with scaled harmonic and anharmonic vibrational wavenumbers and IR intensities of *iso*-C_9H_7NH, 6-*iso*-HC_9H_7N, and 7-*iso*-HC_9H_7N predicted with the B3LYP/6-311++G(d, p) metho

Mode	Sym.	*iso*-C_9H_7NH (group A)				6-*iso*-HC_9H_7N (group B)				7-*iso*-HC_9H_7N (group C)			
		Scaled harm.[a]	Anharmonic	Experiment		Scaled harm.[a]	Anharmonic	Experiment		Scaled harm.[a]	Anharmonic	Experiment	
ν_1	a'	3518 (107)[b]	3476 (58)[b]	3495.2	(105)[c]	3071 (20)	3054 (17)	3059.0	[d]	3069 (27)	3028 (4)	[f]	
				3491.0	(45)								
ν_2	a'					3067 (27)	3041 (29)	3045.1	[d]	3065 (20)	3046 (19)	[f]	
ν_3	a'	3101 (12)	3071 (9)	[f]		3059 (10)	3032 (32)	3025.3	[d]	3059 (17)	3044 (41)	3057.8	[d]
ν_4	a'	3083 (15)	3074 (13)	[f]									
ν_5	a'					3048 (14)	3017 (9)	[f]					
ν_6	a'	3066 (27)	3051 (43)	[f]		3030 (25)	3014 (10)	[f]		3028 (20)	3000 (12)	3025.6	[d]
ν_7	a'					2850 (39)	2808 (4)	2826.4	(69)[c]	2849 (48)	2759 (6)	(HCl)[f]	
ν_8	a'	3050 (10)	3006 (1)	[f]						1641 (2)	1624 (0)	1617.2	(11)[c]
ν_9	a'	1614 (48)	1603 (31)	1613.9	(81)	1560 (25)	1550 (19)	1557.5	(35)	1553 (35)	1542 (16)	1551.2	(69)
ν_{10}	a'	1577 (20)	1565 (6)	1574.4	(18)								
ν_{11}	a'					1450 (22)	1440 (16)	1446.8	(46)				
ν_{12}	a'	1489 (11)	1484 (10)	1490.2	(13)					1435 (10)	1430 (3)	(D)[f]	
ν_{13}	a'	1478 (25)	1465 (2)	1476.6	(58)	1419 (11)	1420 (1)	(A)[f]					
ν_{14}	a'	1440 (17)	1436 (10)	1440.5	(44)								
ν_{15}	a'	1411 (14)	1400 (7)	1420.7	(20)								
ν_{16}	a'					1337 (8)	1322 (8)	1334.1	(18)	1334 (4)	1319 (4)	1331.5	(29)
ν_{17}	a'					1282 (13)	1282 (10)	1284.5	(52)	1286 (10)	1283 (1)	1284.3	(51)
ν_{20}	a'					1185 (7)	1186 (4)	1184.4	(22)	1208 (11)	1201 (5)	1205.1	(14)
ν_{21}	a'	1181 (22)	1165 (14)	1180.9	(33)								
ν_{23}	a'					1048 (5)	1047 (4)	1041.5?	(8)				
ν_{24}	a'	1115 (10)	1114 (16)	1115.3	(13)					1016 (4)	1017 (3)	1017.9	(11)
ν_{25}	a'	1026 (6)	1026 (5)	1022.0	(8)					914 (6)	914 (5)	907.6	(8)
ν_{26}	a'	982 (90)	980 (61)	988.3	(100)	884 (21)	885 (19)	890.9	(54)	883 (12)	884 (11)	892.0	(60)
ν_{27}	a'	932 (5)	937 (14)	939.2	(17)								
ν_{33}	a'					2840 (13)	2755 (18)	2802.5	(49)	2838 (15)	2753 (21)	(HCl)[f]	
ν_{36}	a"									935 (3)	958 (3)	935.4?	(11)
ν_{37}	a"					920 (9)	931 (2)	921.1	(25)	912 (12)	911 (13)	908.4	(51)
ν_{38}	a"	761 (49)	760 (67)	763.1	(66)								
ν_{39}	a"	735 (77)	737 (17)	737.3	(78)	812 (36)	815 (30)	810.2	(100)	821 (45)	828 (38)	817.5	(100)
ν_{41}	a"					698 (24)	700 (26)	697.0	(36)	694 (0)	715 (4)	720.9?	
ν_{42}	a"	571 (17)	550 (15)	577.2	(6)	686 (6)	689 (4)	688.8	(29)	681 (13)	667 (7)	682.2	(46)

[a] Harmonic vibrational wavenumbers scaled according to 0.9122 *x* + 174.3 for wavenumbers >2000 cm^{-1} and 0.9823 x + 0.6 for wavenumbers <2000 cm^{-1}. [b] IR intensities in km mol^{-1}. [c] IR intensities as per cent of that of the most intense line in each species. [d] Severe interference of parent absorption lines intricate the estimation of observed IR intensities. [f] Interference due to absorption of parent or products; in the latter case, the group number of the interfering line or HCl are indicated in parentheses.

Table 5 Comparison of observed vibrational wavenumbers (in cm^{-1}) and relative IR intensities of lines in groups D−F with scaled harmonic and anharmonic vibrational wavenumbers and IR intensities of 8-, 4-, and 5-*iso*-HC_9H_7N predicted with the B3LYP/6-311++G(d, p) method

Mode	Sym.	8-*iso*-HC_9H_7N (group D)			4-*iso*-HC_9H_7N (group E)			5-*iso*-HC_9H_7N (group F)		
		Scaled harm.[a]	Anharmonic	Experiment	Scaled harm.[a]	Anharmonic	Experiment	Scaled harm.[a]	Anharmonic	Experiment
ν_1	a'	3080 (16) [b]	3092 (21) [b]	3083.9 [c]	3083 (18)	3041 (21)	3087.9 [c]	3080 (16)	3082 (10)	3083.2 [c]
ν_2	a'	3070 (35)	3062 (4)	3076.6 [c]	3070 (21)	3068 (24)	[e]	3070 (17)	3054 (15)	[e]
ν_3	a'							3064 (26)	3038 (36)	[e]
ν_5	a'	3046 (17)	3007 (23)	[e]						
ν_6	a'	3024 (25)	2976 (12)	[e]	3026 (25)	3012 (24)	[e]	3031 (22)	2995 (10)	[e]
ν_7	a'	2874 (20)	2838 (5)	(HCl)[e]	2874 (29)	2832 (7)	(HCl)[e]	2874 (26)	2841 (7)	(HCl)[e]
ν_8	a'	1585 (52)	1569 (32)	1576.2 [c]				1582 (18)	1568 (10)	[e]
ν_{10}	a'				1511 (10)	1493 (5)	[e]			
ν_{11}	a'	1472 (14)	1464 (13)	1467.6 (85)[d]	1485 (11)	1477 (8)	1483.7 (20)[d]			
ν_{12}	a'	1431 (19)	1425 (4)	1432.2 (43)				1426 (10)	1415 (5)	(A)[e]
ν_{13}	a'				1417 (11)	1398 (10)	(A)[e]	1418 (14)	1396 (6)	1402.0 (45)[d]
ν_{17}	a'				1274 (10)	1270 (2)	1269.4 (14)			
ν_{18}	a'	1259 (10)	1249 (7)	1245.5 (24)	1249 (25)	1239 (21)	1245.9 (34)			
ν_{20}	a'							1202 (10)	1200 (9)	1201.3 (42)
ν_{25}	a'	935 (17)	937 (15)	941.6 (29)						
ν_{33}	a"	2875 (10)	2796 (14)	(HCl)[e]	2877 (11)	2794 (15)	(HCl)[e]	2875 (11)	2797 (15)	(HCl)[e]
ν_{39}	a"	834 (39)	835 (31)	830.5 (62)	782 (21)	815 (2)	[e]	823 (30)	825 (23)	821.9 (67)
ν_{40}	a”				746 (64)	748 (65)	748.1 (100)			
ν_{41}	a"							710 (15)	709 (9)	708.6 (50)
ν_{42}	a"	654 (43)	657 (38)	653.7 (100)				651 (45)	653 (39)	652.3 (100)

[a] Harmonic vibrational wavenumbers scaled according to $0.9122\,x + 174.3$ for wavenumbers >2000 cm^{-1} and $0.9823\,x + 0.6$ for wavenumbers <2000 cm^{-1}. [b] IR intensities in km mol^{-1}. [c] Severe interference of parent absorption lines intricate the estimation of observed IR intensities. [d] IR intensities as per cent of that of the most intense line in each species. [e] Interference due to absorption of parent or products; in the latter case, the group number of the interfering line or HCl are indicated in parentheses.

Table 6 Comparison of observed vibrational wavenumbers (in cm^{-1}) and relative IR intensities of lines in groups G and H with scaled harmonic and anharmonic vibrational wavenumbers and IR intensities of C_9H_8N predicted with the B3LYP/6-311++G(d, p) method

Mode	Sym.	1-*iso*-HC_9H_7N (group G)			3-*iso*-HC_9H_7N (group H)		
		Scaled harm.[a]	Anharmonic	Experiment	Scaled harm.[a]	Anharmonic	Experiment
ν_1	a'	3083 (17)[b]	3068 (6)[b]	[d]	3085 (16)[b]	3072 (22)[b]	[d]
ν_2	a'	3076 (21)	3052 (8)	[d]	3072 (21)	3047 (21)	[d]
ν_3	a'	3070 (15)	3076 (44)	[d]			[d]
ν_4	a'				3054 (20)	3004 (12)	
ν_6	a'	3012 (37)	2988 (53)	[d]	2985 (35)	2922 (26)	[d]
ν_7	a'	2884 (18)	2827 (15)	(HCl)[d]	2864 (42)	2789 (23)	(HCl)[d]
ν_8	a’				1644 (57)	1623 (35)	1642.7 (100)[c]
ν_{10}	a’				1538 (11)	1530 (7)	[d]
ν_{13}	a’	1414 (14)	1398 (31)	1416.6 (19)[c]			
ν_{19}	a’				1227 (14)	1223 (7)	[d]
ν_{23}	a’				1034 (10)	1032 (9)	(A)[d]
ν_{25}	a'	945 (10)	942 (12)	(D)[d]			
ν_{26}	a'	920 (16)	920 (61)	918.3 (14)	870 (32)	871 (26)	876.4 (60)
ν_{27}	a'						
ν_{35}	a"				970 (11)	968 (8)	[d]
ν_{40}	a"	772 (63)	773 (236)	769.2 (100)	748 (64)	752 (41)	(E)[d]
ν_{41}	a"	715 (7)	729 (122)	714.6 (33)	724 (10)	717 (16)	(C)[d]
ν_{42}	a"	699 (15)	698 (38)	(B)[d]			

[a] Harmonic vibrational wavenumbers scaled according to $0.9122\,x + 174.3$ for wavenumbers >2000 cm^{-1} and 0.9823 x + 0.6 for wavenumbers <2000 cm^{-1}. [b] IR intensities in km mol^{-1}. [c] IR intensities as per cent of that of the most intense line in each species. [d] Interference due to absorption of parent or products; in the latter case, the group number of the interfering line or HCl are indicated in parentheses.

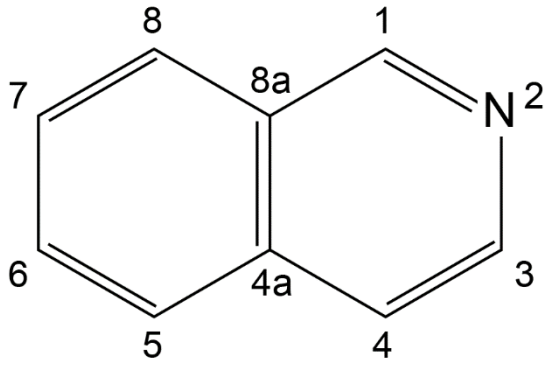

Fig. 1 Numbering of carbon and nitrogen atoms in isoquinoline (*iso*-C_9H_7N) according to IUPAC nomenclature.

(single column)

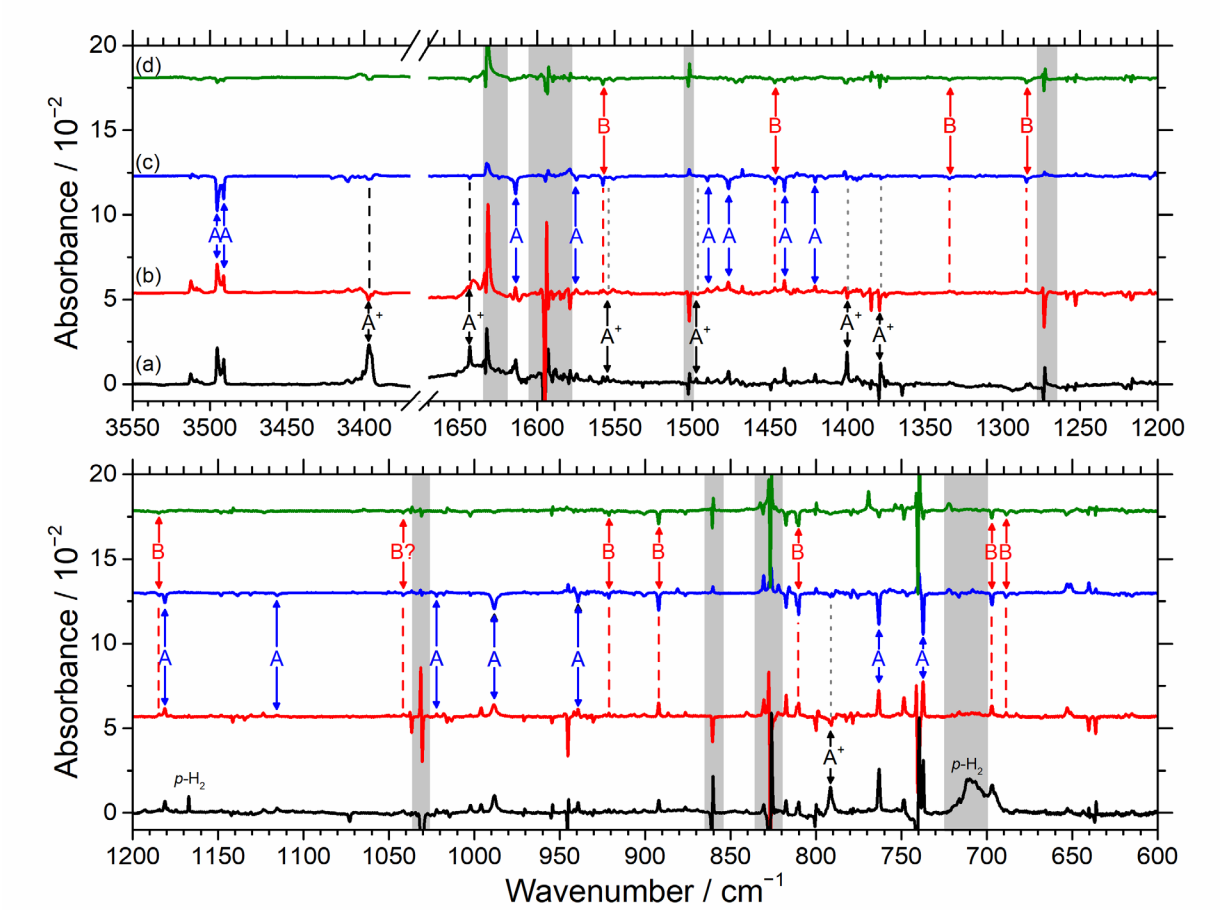

Fig. 2 Infrared spectra of an electron-bombarded *iso*-C_9H_7N/*p*-H_2 matrix after each experimental step. (a) After deposition at 3.2 K for 7 h. The lines of *iso*-C_9H_7N were stripped using a spectrum of a *iso*-C_9H_7N/*p*-H_2 matrix without electron bombardment. (b) Difference spectrum after maintenance of the matrix in darkness for 10 h. (c) Difference spectrum after secondary irradiation at 365 nm for 25 min. (d) Difference spectrum after further irradiation at 405 nm for 3 h. The lines in groups A^+, A, and B are indicated with labels and arrows. Spectral regions subjected to interference from intense absorption of *iso*-C_9H_7N are shaded gray. Baselines were shifted for clarity.

(double column)

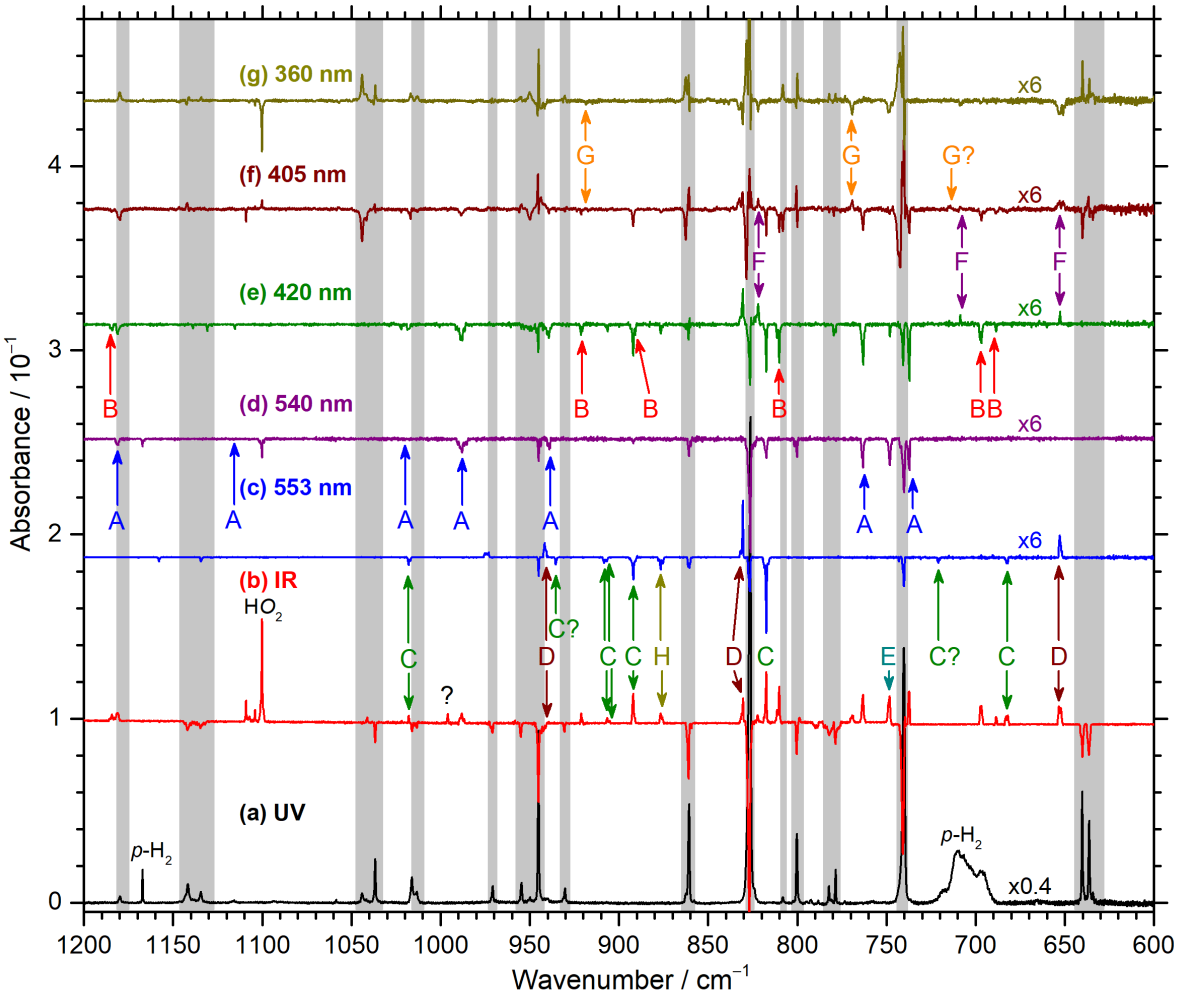

Fig. 3 IR spectra of an *iso*-$C_9H_7N/Cl_2/p$-H_2 matrix in region 1200−600 cm^{-1} at various stages of experiments. (a) Spectrum of an *iso*-$C_9H_7N/Cl_2/p$-H_2 matrix deposited at 3.2 K for 8 h and irradiated at 365 nm for 1 h. (b) Difference spectrum of the matrix after subsequent irradiation with IR light for 2 h. (c) Difference spectra of the matrix upon secondary irradiation at 553 nm for 30 min. (d) Difference spectra of the sample upon secondary irradiation at 540 nm for 30 min. (e) Difference spectra of the sample upon secondary irradiation at 420 nm for 30 min. (f) Difference spectra of the sample upon secondary irradiation at 405 nm for 30 min. (g) Difference spectra of the sample upon secondary irradiation at 360 nm for 30 min. Lines in groups A (*iso*-C_9H_7NH), B (6-*iso*-HC_9H_7N), C (7-*iso*-HC_9H_7N), D (8-*iso*-HC_9H_7N), E (4-*iso*-HC_9H_7N), F (5-*iso*-HC_9H_7N), G (1-*iso*-HC_9H_7N), and H (3-*iso*-HC_9H_7N) are indicated. Spectral regions subjected to interference from intense absorption of *iso*-C_9H_7N are shaded gray. Baselines were shifted for clarity.

(double column)

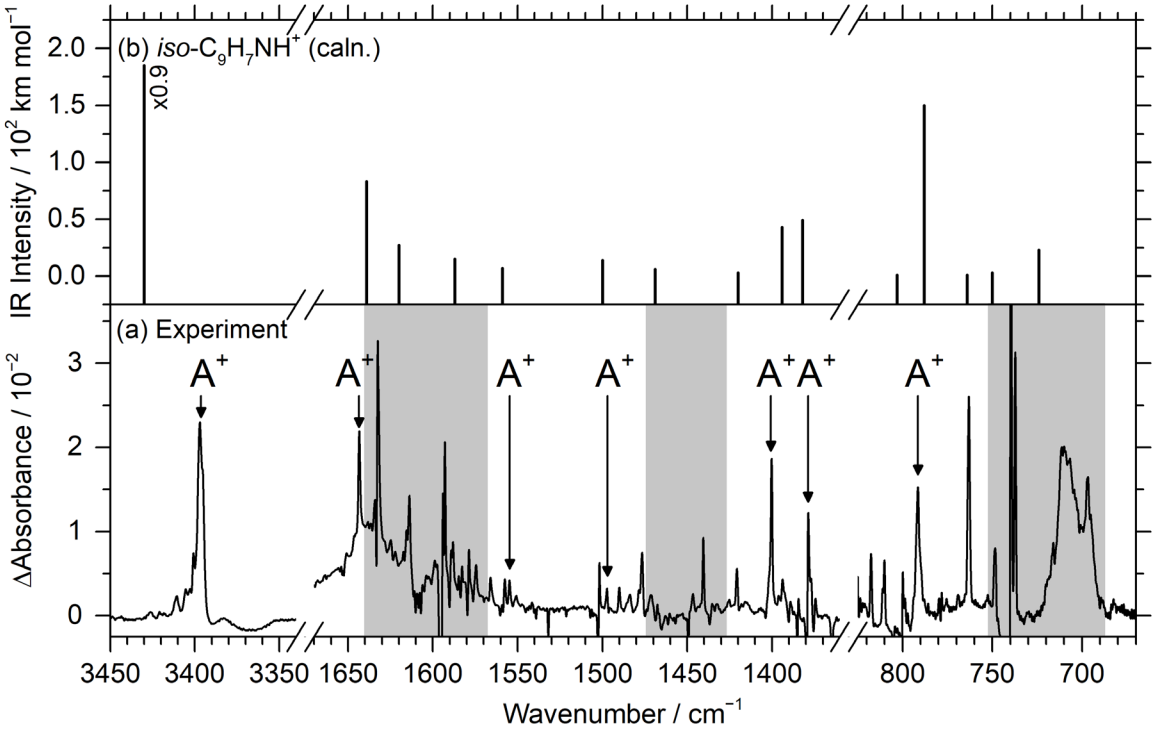

Fig. 4 Comparison of observed lines of group A^+ with predicted IR stick spectrum of *iso*-$C_9H_7NH^+$. (a) The spectrum after deposition; lines of *iso*-C_9H_7N are stripped. Lines in group A^+ are indicated with labels and arrows. Gray rectangles indicate spectral regions suffering from severe interference from parent (*iso*-C_9H_7N). (b) Simulated IR stick spectrum of *iso*-$C_9H_7NH^+$ according to scaled harmonic wavenumbers and IR intensities predicted with the B3LYP/6-311++G(d,p) method.

(double column)

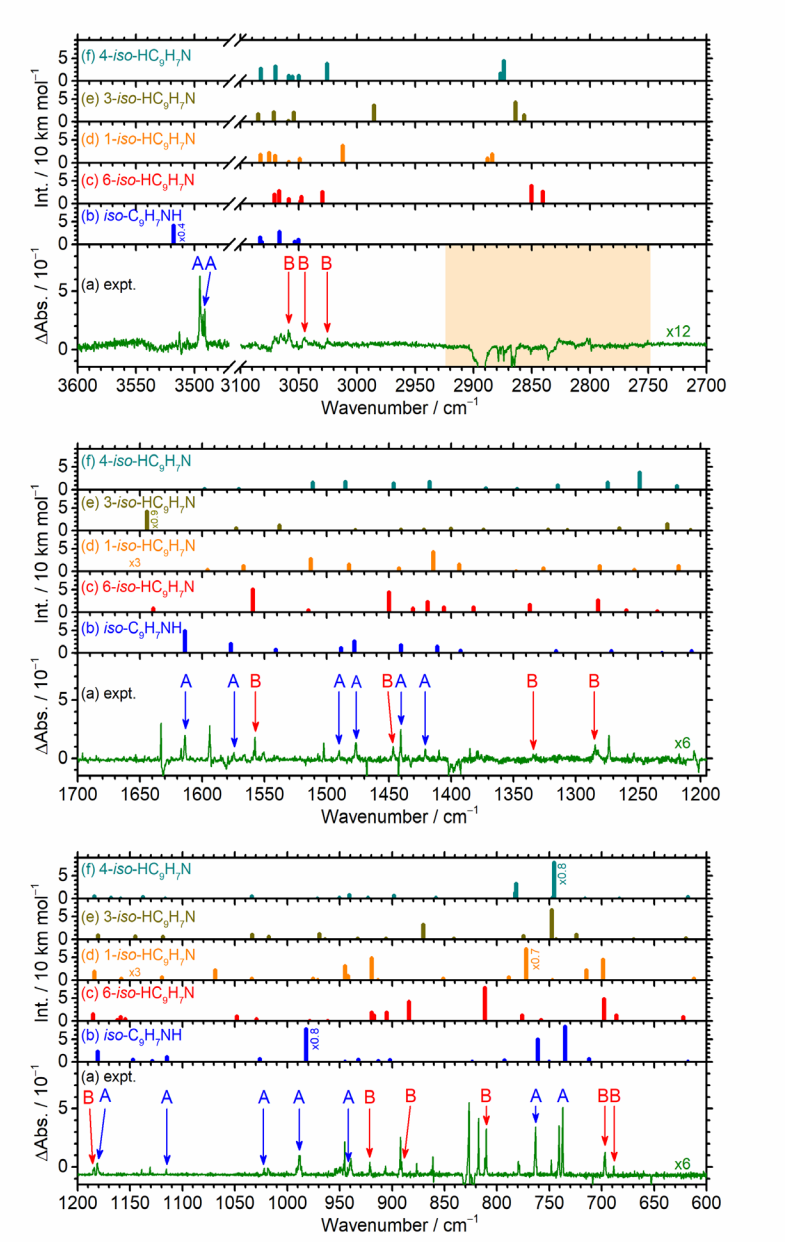

Fig. 5 Comparison of observed lines of groups A and B in *iso*-$C_9H_7N/Cl_2/p$-H_2 experiments with IR stick spectra of *iso*-C_9H_8N predicted with theory. (a) Difference spectrum after irradiation at 420 nm (inverted Fig. 3e); lines belonging to groups A (*iso*-C_9H_7NH) and B (6-*iso*-HC_9H_7N) are indicated with blue and red labels and arrows. IR stick spectra of *iso*-C_9H_7NH (b), 6-*iso*-HC_9H_7N (c), 1-*iso*-HC_9H_7N (d), 3-*iso*-HC_9H_7N (e), and 4-*iso*-HC_9H_7N (f) simulated according to scaled harmonic vibrational wavenumbers and harmonic IR intensities predicted with the B3LYP/6-311++G(d,p) method are presented. Spectral regions that suffer severe interference from absorption of HCl and HCl complexed with water are shaded with light orange.

(double column)

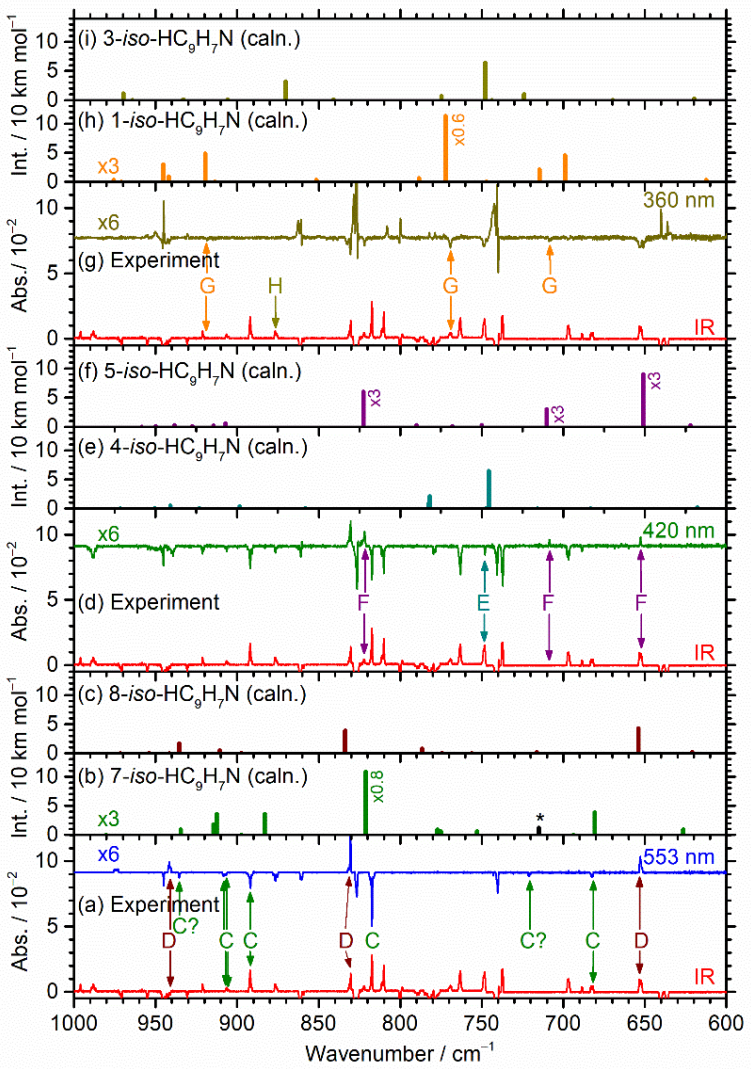

Fig. 6 Comparison of observed lines of groups C to H produced from IR irradiation of an *iso*-$C_9H_7N/Cl_2/p$-H_2 matrix with theoretically predicted stick spectra of representative isomers of hydrogenated isoquinoline (*iso*-HC_9H_7N). (a) Difference spectra after IR irradiation (lower trace, from Fig. 3c) and after secondary photolysis at 553 nm (upper trace, from Fig. 3d); lines of groups C and D are indicated. IR stick spectrum of 7-*iso*-HC_9H_7N (b) and 8-*iso*-HC_9H_7N (c). (d) Same as in (a) except that the upper trace is from secondary photolysis at 420 nm, Fig. 3e; lines of groups E and F are indicated. IR stick spectrum of 4-*iso*-HC_9H_7N (e) and 5-*iso*-HC_9H_7N (f). (g) Same as in (a) except that the upper trace is from secondary photolysis at 360 nm, Fig. 3g, but is inverted; lines of groups G and H are indicated. IR stick spectrum of 1-*iso*-HC_9H_7N (e) and 3-*iso*-HC_9H_7N (f). All IR stick spectra are shown according to scaled harmonic vibrational wavenumbers and IR intensities predicted with the B3LYP/6-311++G(d,p) method. The mark * indicates anharmonic vibrational wavenumber of 7-*iso*-HC_9H_7N.

(single column)

Graphic abstract

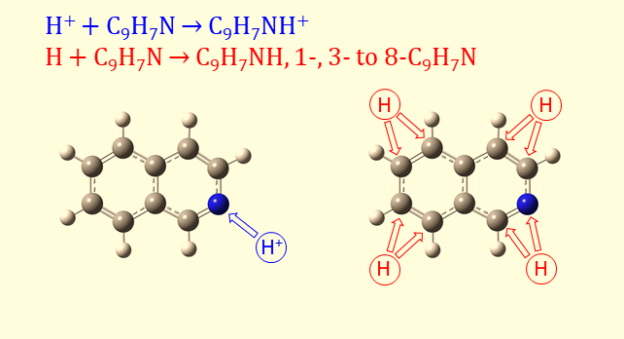

Protonation of isoquinoline was observed at the N-atom site, whereas hydrogenation of isoquinoline was observed at the N-atom site and all C-atom sites except the sharing C atoms on the fused ring.

REFERENCES

[1] S. P. Willner, in *Galactic and Extragalactic Infrared Spectroscopy*, eds. M.F. Kessler and J. P Phillips, D. Reidel Publishing: Dordrecht, 1984, pp. 37–58.

[2] A. G. G. M. Tielens, in *PAHs and the Universe*, eds. C. Joblin and A. G. G. M. Tielens, EAD Sciences: Les Ulis, 2011, pp. 3–10.

[3] A. Leger and J. L. Puget, *Astron. Astrophys.*, 1984**, 137**, L5−L8.

[4] J. L. Puget and A. Léger, *Annu. Rev. Astron. Astrophys.*, 1989, **27**, 161−198.

[5] L. J. Allamandola, A. G. G. M. Tielens and J. R. Barker, *Astrophys. J.*, 1985, **290**, L25−L28.

[6] L. J. Allamandola, A. G. G. M. Tielens and J. R. Barker, *Astrophys. J. Suppl. Ser.*, 1989, **71**, 733−775.

[7] D. M. Hudgins, C. W. Bauschlicher Jr. and L. J. Allamandola, *Spectrochim. Acta A Mol. Biomol. Spectrosc.*, 2001, **57**, 907−930.

[8] O. Dopfer, in *PAHs and the Universe*, eds. C. Joblin and A. G. G. M. Tielens, EAD Sciences: Les Ulis, 2011, pp. 103−108.

[9] M. Bahou, Y.-J. Wu and Y.-P. Lee, *Angew. Chem. Int. Ed.*, 2014, **53**, 1021–1024.

[10] M. Tsuge, M. Bahou, Y.-J. Wu, L. J. Allamandola and Y.-P. Lee, *Astrophys. J.*, 2016, **825**, 96.

[11] P. Sundararajan, M. Tsuge, M. Baba and Y.-P. Lee, *ACS Earth Space Chem.*, 2018, **2**, 1001−1010.

[12] M. Tsuge, C.-Y. Tseng and Y.-P. Lee, *Phys. Chem. Chem. Phys.*, 2018, **20**, 5344–5358.

[13] E. Peeters, S. Hony, C. V. Kerckhoven, A. G. G. M. Tielens, L. J. Allamandola, D. M. Hudgins and C. W. Bauschlicher, *Astron. Astrophys.*, 2002, **390**, 1089−1113.

[14] C. Boersma, J. D. Bregman and L. J. Allamandola, *Astrophys. J.*, 2013, **769**, 117.

[15] A. Ricca, C. Boersma and E. Peeters, *Astrophys. J.*, 2021, **923**, 202.

[16] M. P. Bernstein, A. L. Mattioda, S. A. Sandford and D. M. Hudgins, *Astrophys. J.*, 2005, **626**, 909−918.

[17] Z. Peeters, O. Botta, S. B. Charnley, Z. Kisiel, Y.-J. Kuan and P. Ehrenfreund, *Astron. Astrophys.*, 2005, **433**, 583−590.

[18] P. G. Stoks and A. W. Schwartz, *Geochim. Cosmochim. Acta*, 1981, **45**, 563–569.

[19] P. G. Stoks and A. W. Schwartz, *Geochim. Cosmochim. Acta*, 1982, **46**, 309–315.

[20] J. Bouwman, A. Bodi and P. Hemberger, *Phys. Chem. Chem. Phys.*, 2018, **20**, 29910–29917.

[21] E. P. L. Hunter and S. G. Lias, *J. Phys. Chem. Ref. Data*, 1998, **27**, 413–656.

[22] H. Alvaro Galué, O. Pirali and J. Oomens, *Astron. Astrophys.*, 2010, **517**, A15.

[23] M. Tsuge and Y.-P. Lee, in *Molecular and Laser Spectroscopy*, eds. V. P. Gupta and Y. Ozaki Elsevier, 2020, pp. 167−215.

[24] M. Bahou, P. Das, Y.-F. Lee, Y.-J. Wu and Y.-P. Lee, *Phys. Chem. Chem. Phys.*, 2014, **16**, 2200–2210.

[25] C.-Y. Tseng, Y.-J. Wu and Y.-P. Lee, *J. Phys. Chem. A*, 2022, **126**, 2361–2372.

[26] P. Sundararajan, M. Tsuge, M. Baba, H. Sakurai and Y.-P. Lee, *J. Chem. Phys.*, 2019, **151**, 044304.

[27] M. Bahou, Y.-J. Wu and Y.-P. Lee, *Phys. Chem. Chem. Phys.*, 2013, **15**, 1907–1917.

[28] C. S. Hansen, S. J. Blanksby and A. J. Trevitt, *Phys. Chem. Chem. Phys.*, 2015**, 17**, 25882–25890.

[29] G. Féraud, L. Domenianni, E. Marceca, C. Dedonder-Lardeux and C. Jouvet, *J. Phys. Chem. A*, 2017, **121**, 2580–2587.

[30] S. Tam and M. E. Fajardo, *Appl. Spectrosc.*, 2001, **55**, 1634–1644.

[31] I. F. Silvera, *Rev. Mod. Phys.*, 1980, **52**, 393–452.

[32] M. E. Fajardo, *Appl. Spectrosc.*, 2019, **73**, 1403–1408.

[33] M. J. Frisch, G. W. Trucks and H. B. Schlegel, *et al*., *Gaussian 16 Rev. B.01*, Gaussian Inc., Wallingford, CT, 2016.

[34] A. D. Becke, *J. Chem. Phys.*, 1993, **98**, 5648–5652.

[35] C. T. Lee, W. T. Yang and R. G. Parr, *Phys. Rev. B* 1988, **37**, 785–789.

[36] W. J. Hehre, L. Radom, P. V. R. Schleyer and J. A. Pople, *Ab Initio Molecular Orbital Theory*, Wiley, New York, Vol. 548. 1986.

[37] J. Bloino and V. Barone, *J. Chem. Phys.*, 2012, **136**, 124108.

[38] G. D. Purvis and R. J. Bartlett, *J. Chem. Phys.*, 1982, **76**, 1910−1918.

[39] M. E. Jacox, *J. Phys. Chem. Ref. Data*, 1998, **27**, 115–393.

[40] P. L. Raston and D. T. Anderson, *J. Chem. Phys*., **2007**, 126, 021106, 1–4.

[41] C. S. Hansen, S. J. Blanksby and A. J. Trevitt, *Phys. Chem. Chem. Phys.*, 2015, **17**, 25882–25890.

[42] C. M. King and E. R. Nixon, *J. Chem. Phys.* 1968, **48**, 1685−1695.

[43] E. Peeters, L. J. Allamandola, D. M. Hudgins, S. Hony and A. G. G. M. in *Astrophysics of Dust*, eds. A. N. Witt, G. C. Clayton and B. T. Draine, 2004, **309**, 141.

[44] J. D. Brenner and J. R. Barker, *Astrophys. J.*, 1992, **388**, L39−L43.

[45] A. G. G. M. Tielens, *Annu. Rev. Astron. Astrophys.*, 2008, **46**, 289−337.

[46] D. M. Hudgins and L. J. Allamandola, *Astrophys. J.*, 1999, **516**, L41.

[47] S. Hony, C. Van Kerchhoven, E. Peeters, A. G. G. M. Tielens, D. M. Hudgins and L. J. Allamandola, *Astron. Astrophys.*, 2001, **370**, 1030−1043.